The interactions of fullerene C60 and Benzo(α)pyrene influence their bioavailability and toxicity to zebrafish embryos

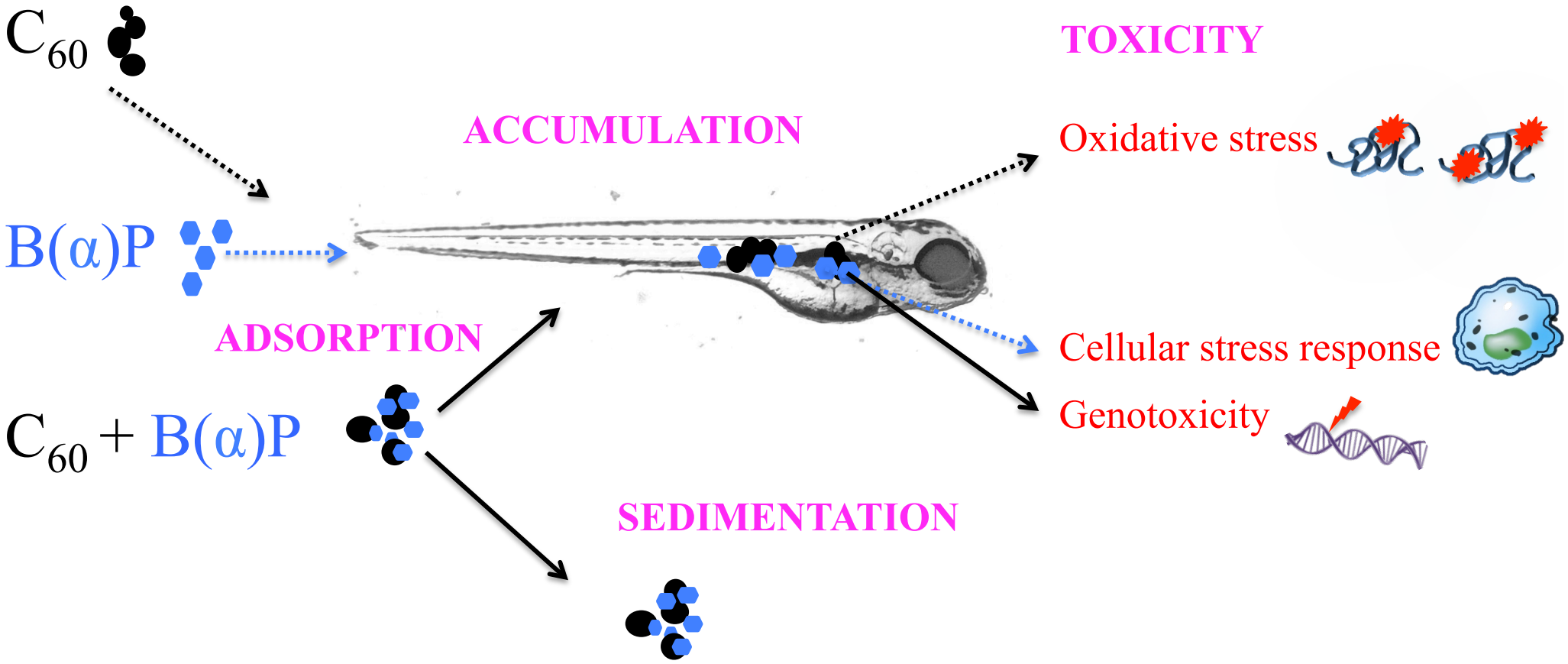
C60
B(α)P
C60 + B(α)P
ACCUMULATION
ADSORPTION
SEDIMENTATION
TOXICITY
Oxidative stress
Cellular stress response
Genotoxicity

The interactions of Fullerene C_{60} and Benzo(α)pyrene influence their bioavailability and toxicity to zebrafish embryos

Camilla Della Torre[1], Daniela Maggioni[2], Anna Ghilardi[1], Marco Parolini[3], Nadia Santo[1], Claudia Landi[4], Laura Madaschi[1], Stefano Magni[1], Stefano Tasselli[5], Miriam Ascagni[1], Luca Bini[4], Caterina La Porta[3], Luca Del Giacco[1], Andrea Binelli[1]

[1]Department of Biosciences, University of Milan, Italy
[2]Department of Chemistry, University of Milan, Italy
[3]Department of Environmental Science and Policy, University of Milan, Italy
[4]Department of Life Science, University of Siena, Italy
[5]CNR-IRSA (National Research Council-Water Research Institute), Brugherio, Italy

Abstract

This study aimed to assess the toxicological consequences related to the interaction of fullerene nanoparticles (C_{60}) and Benzo(α)pyrene (B(α)P) on zebrafish embryos, which were exposed to C_{60} and B(α)P alone and to C_{60} doped with B(α)P. The uptake of pollutants into their tissues and intra-cellular localization were investigated by immunofluorescence and electron microscopy. A set of biomarkers of genotoxicity and oxidative stress, as well as functional proteomics analysis were applied to assess the toxic effects due to C_{60} interaction with B(α)P. The carrier role of C_{60} for B(α)P was observed, however adsorption on C_{60} did not affect the accumulation and localization of B(α)P in the embryos. Instead, C_{60} doped with B(α)P resulted more prone to sedimentation and less bioavailable for the embryos compared to C_{60} alone. As for toxicity, our results suggested that C_{60} alone elicited oxidative stress in embryos and a down-regulation of proteins involved in energetic metabolism. The C_{60} + B(α)P induced cellular response mechanisms similar to B(α)P alone, but generating greater cellular damages in the exposed embryos.

Capsule

Once C_{60} nanoparticles and B(α)P meet in water, they reciprocally affect their bioavailability and, by consequence, their toxicity to organisms.

Keywords: Fullerene nanoparticles; *Danio rerio*; oxidative stress; proteomics; trojan horse effect

1. Introduction

Fullerenes are carbonaceous nanoparticles (NPs) broadly used in several applications including targeted drug delivery systems, lubricants, energy devices, catalysis, surfaces for antiwear applications, cosmetics and sporting goods, due to their outstanding chemico-physical properties (Yadav and Kumar 2008; Mousavi et al., 2017). As a result of the growing production of fullerenes - and especially C_{60}- there is rising concern regarding their presence and impacts on the natural ecosystems. Indeed, fullerenes nanoparticles have been detected in many environmental matrices as atmospheric aerosol (Sanchis et al., 2012) waters (Farrè et al., 2010; Pakarinen et al., 2013; Astefanei et al., 2014), sediments (Sanchis et al., 2015) and soils (Carboni et al., 2016). Therefore, it is extremely important to assess their interactions and toxic effects on wildlife, with particular emphasis on aquatic environments, which act as ultimate sinks for NPs. In fact, the same properties that render fullerenes a unique and innovative material can trigger deleterious effects to natural biocenosis.

The toxicity of C_{60} has been described in bacteria (Freitas Cordiero et al., 2014), crustaceans (Klaper et al., 2009), bivalves (Canesi et al., 2010; Al-Subiai et al., 2012), chironomids (Waissi et al., 2017) and fishes (Ferreira et al., 2012; Gorrochategui et al., 2017) as well as the potential for trophic transfer (Fortner et al., 2010; Chen et al., 2014). Besides its inherent toxicity, C_{60} has also exceptional sorption capacity towards hydrophobic chemicals (Hu et al., 2014; Velzeboer et al., 2014) that may significantly affect their bioavailability, bioconcentration and toxicity. Although some studies showed the ability of C_{60} to sequester diverse contaminants and to reduce their toxicity (Yang et al., 2010; Park et al., 2011), it can conversely act as carrier for organic pollutants enhancing their biological effects on the organisms (Baun etal., 2008; Al-Subiai et al., 2012; Ferreira et al., 2014; Seke et al., 2017; Li et al., 2017). Therefore, the release of C_{60} into the aquatic environment in the presence of toxic chemicals may pose a further risk for ecosystems, with hardly predictable effects.

This study aimed to assess the interactive effects of fullerene NPs (C_{60}) and Benzo(α)pyrene (B(α)P) on zebrafish (*Danio rerio*) embryos. Specifically, we doped C_{60} with B(α)P (C_{60}+B(α)P from now on) and compared the effect on zebrafish embryos exposed to the two contaminants singly administered and to the C_{60} + B(α)P complex. This experimental plan allowed to assess the accumulation and toxicity only of the B(α)P adsorbed on C_{60} without any interference of free hydrocarbon. A thorough evaluation of chemico-physical interactions between the two pollutants has been performed, and the uptake and distribution of C_{60} and B(α)P were shown through advanced microscopy techniques. To evaluate whether C_{60} + B(α)P affects different molecular pathways compared to the two singly administered pollutants, a suite of biomarkers was applied. The activity of proteins involved in the detoxification and antioxidant response, namely glutathione-S-transferase (GST), catalase (CAT) and superoxide dismutase (SOD), was measured, while the oxidative damage was assessed by the measurement of protein carbonylation (PCC). The genotoxicity was assessed by the application of single gel cell electrophoresis (SCGE) assay, DNA diffusion assay and Micronucleus test. Proteomics analysis was also performed to evaluate changes of embryos proteome profile, and suggesting possible mechanisms of action of the pollutants, both alone or in combination.

2. Materials and Methods

2.1 Materials

C_{60} (CAS number: 99685-96-8) and all reagents used for chemical and biomarker analyses were purchased by Sigma-Aldrich (Steinheim, Germany). B(α)P powder (CAS number: 50-32-8) was supplied by Dr. Ehrenstorfer, (Augsburg, Germany).

2.2 C_{60} characterization

The bulk C_{60} and C_{60} + B(α)P were observed at Zeiss LEO 912ab Energy Filtering TEM operating at 100 kV, at a magnification of 25-50,000x using a CCD-BM/1 K system.

Dynamic Light Scattering (DLS) was used to measure the hydrodynamic diameter (size distribution) and the charges at the surface (ζ-potential) of water suspended C_{60} nanoparticles. The measurements were performed on a Malvern Zetasizer Nano ZS instrument (Malvern instruments, UK) equipped with a device for the ζ-potential measurement, employing a solid state He-Ne laser (633 nm) as a light source and recovering the scattered light at an angle of 173° (Series software – version 7.02 – Particular Sciences, UK).

2.3 B(α)P sorption on C_{60}

Two aliquots of C_{60} (200 mg/L) were suspended in 200 mL of MilliQ water and stirred for 15 days at 20 °C. The first aliquot was doped with 1 mg/L B(α)P dissolved in dimethylsulhpoxide (DMSO), while the second portion was not contaminated. The two suspensions were stirred for 5 days at 20 °C in the dark. They were then centrifuged at 3,000 x g for 30 min. The precipitated C_{60} with B(α)P adsorbed were completely dried in an oven at 40 °C and used for embryos exposures. For measuring the B(α)P fraction remaining solubilized in water, the supernatants were treated with toluene (1:5 v/v, respectively) leaving the mixture under stirring for 90 min at 20 °C in order to extract the free B(α)P solubilized in water by liquid/liquid extraction. The amount of B(α)P in toluene solutions was measured by fluorescence detection, as described in Supplementary Materials. The same technique was used to measure the amount of B(α)P adsorbed on C_{60} NPs. In this case, the samples were prepared by dissolving 5 mg of dried C_{60} + B(α)P in 200 mL toluene. A sample containing 5 mg of untreated C_{60} in 200 mL toluene served as a blank.

2.4 Preparation of C_{60} suspensions and hydrodynamic behaviour in exposure media

The C_{60} and C_{60} + B(α)P were suspended and equilibrated at concentration of 20 mg/L, in zebrafish water (ZFW) for 10 days by stirring in the dark at 20 °C. DLS analysis was performed as described above to determine both hydrodynamic diameters and surface charges (ζ potentials) of each sample.

To evaluate the sedimentation process, the UV−vis absorbance spectra of the two suspensions were aquired on an Agilent model 8543 spectrophotometer at room temperature.

2.5 Zebrafish embryo exposure

Adult zebrafish of the AB strain were bred in the fish facility of the Department of Biosciences (University of Milan), to obtain 1-cell stage embryos. Our facility is strictly compliant with the Italian legislation (Legislative Decree No. 116/92) concerning animal welfare, as also certified by the authorization released by the Milan municipality (Art. 10 of Legislative Decree No. 116, dated 27.1.1992). Animal procedures were carried out in conformity with the relevant guidelines and regulations.

To avoid any physical interference with the uptake of C_{60}, removal of chorion with pronase (0.5 mg/mL) was performed at 24 h post-fertilization (hpf), immediately prior to the exposure. Embryos were then exposed to B(α)P (8 μg/L), C_{60} (20 mg/L) and to C_{60} + B(α)P in Petri dishes in a total volume of 4 mL. B(α)P concentrations were defined based on the effective B(α)P sorption on C_{60} (20 mg/L) measured by emission spectra (see results). A preliminary range-finding assured that concentrations of C_{60} and B(α)P were not able to produce mortality or any morphological embryos alteration. Control embryos were exposed to zebrafish water (ZFW) and to vehicle (0.08% DMSO) only. The exposure proceeded until 96 hpf under semistatic conditions, renewing the exposure solutions every 24 h in new vessels. To prevent embryos pigmentation for B(α)P visualization in tissues, ZFW was added with 0.003% 1-phenyl 2-thiourea (PTU). For biochemical analyses and proteomics, embryos were stored at -80 °C until processing. For advanced microscopy and genotoxicity assessment, embryos were immediately processed at the end of the exposure as described below. Experiments were run at least 3 times for each analysis.

2.6 Electron microscopy

A detailed description of ultrastructural analysis procedures is reported in Binelli et al. (2017). Ten embryos from each experimental group were fixed in a mixture containing 4% paraformaldehyde and 2.5% glutaraldehyde in 0.1 M sodium cacodylate buffered solution (pH 7.4). Then the embryos were postfixed in 1% OsO_4, dehydrated in a graded ethanol series and infiltrated in Araldite-Epon. Ultrathin sections of about 70 nm were obtained by Ultracut E microtome (Reichert, Austria). Counterstain of sections was not performed to avoid interference with C_{60} visualization. Digital images were acquired using a CCD-BM/1K system, and image elaboration was performed using the ESI vision software AnalySIS (Soft Imaging Systems, Muenster, Germany).

2.7 Immunohistochemistry

Details of the procedure are described in Binelli et al. (2017). Briefly, embryos were fixed in paraformaldehyde (4%) and cryo-protected. For immunofluorescence, cryostat sections (10 μm) were incubated with primary antibody anti-polycyclic aromatic hydrocarbons (anti-PAHs 1/100 in PBS, Santa Cruz) and exposed to secondary antibody (Alexa Fluor 488 goat anti-mouse 1:200, Thermo Fisher Scientific). Finally, samples were mounted in PBS/glycerol (1:2 v/v) with DNA-binding dye 40-60-diamidino2-phenylindole (DAPI). Sections were observed by a confocal microscope Leica SP2 microscope equipped with He/Kr and Ar laser (Leica, Wetzlar, Germany).

2.8 Accumulation of C_{60} in zebrafish embryos

The quantification of C_{60} accumulated in zebrafish embryos was performed according to the method described by Waissi et al. (2017), with slight modifications. Embryos were exposed in triplicate to C_{60} and C_{60} + B(α)P and to ZFW only (N = 160 for each treatment). After 96 hpf, embryos were collected and washed with MilliQ water, then homogenized in 1 mL of 2% NaCl solution. Toluene (1 mL) was added, the solution vortexed and transferred in an ultrasonic bath for 15 min. After sedimentation, the toluene fraction was collected and C_{60} absorbance was measured at 335 nm using a Jenway spectrophotometer (Stone, UK). The baseline absorbance detected in controls was

158 subtracted to absorbance of C_{60} samples. The C_{60} concentration was determined based on standard
159 curve (0.01-10 μg/mL $r^2 = 0.9997$).
160
161 2.9 Biomarkers analyses
162 A detailed description of biomarkers analysis is reported in Supplementary Materials. The GST,
163 SOD and CAT activities were analysed on homogenates obtained from pools of 60 embryos for
164 each treatment. PCC was evaluated on homogenates obtained from pools of 80 embryos.
165 Genotoxicity was performed on cells dissociated from a pool of 10 zebrafish embryos (three pools
166 per treatment) according to the methods described in Parolini et al. (2017). Briefly, cell viability
167 was assessed by the trypan blue dye exclusion method. The percentage of DNA in the comet tail
168 and the ratio between migration length and comet head diameter (LDR) were used as endpoints of
169 primary genetic damages. The apoptotic and necrotic cell frequency and the frequency of
170 micronuclei (MN‰) were measured as fixed genetic damage.
171
172 2.10 Functional proteomics
173 The analysis was performed on pools of 90 embryos for each experimental group. A detailed
174 description of the procedure is reported by Binelli et al. (2017). Briefly, 200 μg of protein for each
175 group were precipitated using a chloroform/methanol/water mixture (4:1:3 v/v). Proteins
176 resuspended in rehydratation (denaturing) buffer were loaded in 18 cm pH 3–10 non-linear gradient
177 IPG strips (GE Healthcare, Milan, Italy) and IEF was performed on the Ettan IPGphor II system
178 (GE Healthcare, USA). Protein separation in the second dimension was performed on 12%
179 acrylamide gel in an Ettan DALTsix electrophoretic unit (GE Healthcare, UK). Gels were died by
180 silver stain (ProteoSilver Plus Silver Stain kit; Sigma Aldrich, Milan, Italy), according to producer
181 instructions. Gel images were analyzed by the ImageMaster 2D Platinum software (Amersham
182 Biosciences, USA). Significant protein differences were investigated comparing gels from controls
183 group (ZFW, DMSO) with those from treatment groups. Spots were statistically evaluated in terms

of the mean relative volume (vol.%) using Student's t-test for unpaired samples taking $p<0.05$ as significant treshold. A further criterion for differential regulation was employed such as minimum 2-folds change cut-off relative to controls. Significantly modified protein spots were excised from gels, destained, dehydrated with acetonitrile and digested with trypsine (Sigma Aldrich, Milan, Italy). The proteins were identified by MALDI TOF-TOF (matrix-assisted laser desorption/ionization time of flight) mass spectrometry analysis; the Peptide Mass Fingerprinting (PMF) was performed using an Ultraflex III MALDI-TOF/TOF mass spectrometer (Bruker Daltonics, Billerica, MA, United States). Spectra were analyzed by the Flex Analysis software v.3.0. Mascot (Matrix Science Ltd., London, UK, http://www.matrixscience.com). On-line-available software was used for PMF search in NCBInr or Swiss-Prot/TrEMBL databases with taxonomy set for *Danio rerio*.

2.11 Statistical analysis

Biomarker data were investigated through one-way analysis of variance (ANOVA) after checking for normality and homoscedasticity, taking $p<0.05$ as significance cut-off. The ANOVA was followed by the Duncan's *post-hoc* test to investigate significant differences between exposure groups. The analyses were performed using the STATISTICA 7.0 software package.

3. Results and Discussion

3.1 C_{60} characterization

The bulk C_{60} consisted mostly of isometric NPs, with mean diameter estimated by TEM micrographs of about 35.6 ± 10.9 nm and few submicrometric aggregates. A similar structure was observed also for C_{60} + B(α)P (Fig. S1). The DLS analysis of C_{60} suspension in MilliQ water (1 mg/mL) showed the presence of a homogeneous population of NPs aggregates with hydrodynamic radius of 519 ± 169 nm, and polydispersion index (PDI) of 0.39. The stability of the suspension was

209 confirmed by the highly negative surface charge value (-36 ± 1 mV) derived from a ζ-potential
210 measurement.
211 In ZFW, the Z average measured for C_{60} suspension (20 mg/L) was 899 ± 97 nm with PDI of 0.376,
212 indicating the presence of homogeneous population of NPs (trace red in Fig. 1A). On the contrary,
213 the suspension of C_{60} + B(α)P showed the presence of two aggregate populations, centered at 767 ±
214 44 nm and 189 ± 13 nm (trace blue in Fig. 1A) showing also the presence of smaller aggregates.
215 Nevertheless, the counts per second of scattered light in this second set of measurements resulted
216 very poor, indicating that a very quick sedimentation phenomenon occurred. Indeed, the suspension
217 just after the DLS measurement pointed out evident sediment at the bottom of the cuvette (Fig. S2).
218 Moreover, UV-Vis analysis highlighted also a significant sedimentation of C_{60} + B(α)P with respect
219 to C_{60} alone, leading to a decrease of concentration of the suspended NPs in ZFW (Fig. 1B). These
220 results suggested that once contaminated with B(α)P, C_{60} NPs were more prone to aggregation and
221 to be easily settled out of suspension.
222 Finally, the ζ potential value of C_{60} alone was -23.4 ± 0.2 mV, and a similar value was measured for
223 C_{60} combined with B(α)P, equal to -21.6 ± 0.3 mV.
224
225 3.2 B(α)P sorption on C_{60}
226 A small fraction (2.9 %) of the administered B(α)P was recovered in the water phase after 5 days of
227 contamination, while a marked amount of B(α)P (38%) was adsorbed on C_{60}, equal to 378 μg/g.
228 Based on these results, the concentration of B(α)P corresponding to suspensions containing 20
229 mg/L of C_{60} was set to 8 μg/L. These results confirmed the sorption capacity of C_{60} towards B(α)P
230 in the water media as reported for other PAHs (Baun et al., 2008; Hu et al., 2014). Such findings
231 highlighted that C_{60} could alter significantly the fate and transport of B(α)P in the aquatic
232 ecosystems. Moreover our results suggest that as B(α)P is relatively stable and can move in the
233 atmosphere for a long time, it can bind to atmospheric NP such as C_{60}, and be subsequently
234 introduced in the water environment. The high sedimentation rate observed for the complex C60 +

B(α)P strongly suggests that a relevant fraction of the hydrocarbon adsorbed on C_{60} could reach and accumulate in the sediments.

3.3 Accumulation of C_{60}

The measurement of C_{60} body burden showed a higher accumulation in embryos exposed to C_{60} alone (16.32 ± 6.45 ng/embryo, corresponding to three-fold increase) than C_{60} contaminated with B(α)P (3.90 ± 3.39 ng/embryo). Therefore, the observed increase of C_{60} sedimentation due to B(α)P adsorption reduced the NPs bioavailability and uptake by the embryos. This result highlight that, in natural conditions, the presence of contaminants in water could significantly influence the environmental fate of C_{60}, potentially enhancing its distribution in sediments. According with our result, a previous study on zebrafish embryos showed that the combination of C_{60} and Hg^{2+} increased NPs size and sedimentation, resulting in a lower accumulation of NPs in embryos, compared to the C_{60} alone (Henry et al., 2013). Similarly, two other studies on nano-TiO_2 in combination with metals have suggested that chemico-physical interactions (e.g. adsorption) between NPs and contaminants can significantly alter their accumulation in organisms (Pavagadhi et al., 2014; Fan et al., 2016).

TEM observations showed a microvilli-mediated internalization of C_{60} NPs in enterocytes mediated (Fig. 2A). The adsorption of B(α)P on C_{60} did not modify this behavior, as also doped NPs entered enterocytes, (Fig. 2B). TEM observations confirmed the ability of C_{60} to pass through the gill cell membranes and accumulate in the epithelium cells (Fig. 2C).

3.4 B(α)P accumulation

The B(α)P fluorescence signal was detected in gills (Fig. 3C, D) and in the gastrointestinal tract (Fig. 3F, G) of embryos exposed to the hydrocarbon. A similar pattern was revealed also in C_{60} + B(α)P exposed embryos, showing that C_{60} can act as carrier for the adsorbed B(α)P. Confocal observations suggested that the B(α)P adsorbed on C_{60} enters the organism mostly through the

gastrointestinal tract, where it can be released and transferred to other compartments as described for different carbon nanomaterials (CNMs; Wang et al. 2011; Su et al., 2013; Seke et al., 2017). Nevertheless, the mechanisms determining the release of contaminants from CNMs and distribution in the organism are still barely understood, and might vary depending on the CNM. For instance, in our recent study we showed that the B(α)P sorbed on carbon nanopowder (CNPW) was taken up by zebrafish embryos and it followed the physical contaminant distribution rather than its natural accumulation (Binelli et al., 2017). On the contrary, the immunoistochemistry analysis showed that the adsorption on C_{60} did not affect the embryo B(α)P distribution. It is known that fullerene structures, as well as other allotropic carbon-based materials like carbon nanotubes (CNT), interact with the aromatic moieties of many different molecules by π-π interactions (Lu et al., 2006). Yet the sorption of aromatic hydrocarbons by C_{60} has been calculated and compared with the ability of CNTs to absorb these small molecules (Huffer et al., 2017), concluding that the sorption by CNTs is stronger than that by C_{60} and may be attributable, among others, to the smaller surface area of the fullerene aggregates in water with respect to the ones of other CNMs (Yang et al., 2006). Therefore, the small difference in the biodistribution of B(α)P when administered alone or associated to C_{60}, could be due to a faster equilibrium release from this material with respect to the dissociation from other carbon-based materials in the physiological environment as the gastrointestinal fluids.

3.5 Effects of C_{60}

No mortality or teratogenic effects have been recorded in zebrafish embryos exposed to contaminants alone or in combination. Concerning the oxidative stress biomarkers, exposure to B(α)P determined a significant inhibition of CAT activity compared to DMSO ($p < 0.0001$), but did not affect SOD activity. A significant increase of SOD ($p = 0.0004$) and CAT ($p = 0.01$) activities was observed in embryos exposed to C_{60} alone. On the other hand, the activity of the two enzymes was restored to control levels following C_{60} + B(α)P exposure, resulting significantly lower in respect to C_{60} alone ($p = 0.0003$ for SOD and $p = 0.0013$ for CAT) (Fig. 4A,B). The measurement

286 of protein carbonylation showed an increase in carbonyl content exclusively in embryos exposed to
287 C_{60} alone compared to controls ($p = 0.019$; Fig. 4D).
288 The increase of SOD and CAT activity confirmed the ability of C_{60} to induce antioxidant response,
289 as already pointed out in other studies performed on several aquatic models (Usenko et al., 2008;
290 Klaper et al. , 2009; Ferreira et al., 2012; Waissi et al., 2017; Lv et al., 2017). The oxidative stress
291 generated by C_{60} was also confirmed by the increase of protein carbonylation -marker of oxidative
292 damage- observed in embryos exposed to C_{60} alone. Indeed, the carbonylation of proteins involved
293 in various cellular mechanisms has been described, as consequence of the oxidative stress generated
294 following exposure to NPs (Driessen et al., 2015). On the contrary, there was no evidence of
295 oxidative damage in co-exposure, and a significant reduction of the activity of antioxidant enzymes
296 was observed in comparison to the single pollutant. This result is likely related to the lower
297 accumulation of C_{60} observed in embryos exposed to the B(α)P doped NPs in respect to C_{60} alone,
298 therefore unable to induce a measurable cellular response.
299 A significant increase of GST activity was observed in embryos exposed to B(α)P ($p = 0.012$) and
300 C_{60} ($p = 0.0002$ vs control) administered alone. GST is involved in phase II of
301 metabolism/detoxification catalyzing the conjugation of glutathione to several environmental
302 pollutants and oxidative stress by-products (van der Oost et al., 2003). The induction of GST
303 activity upon exposure to C_{60} alone confirmed the active role of this enzyme in the cellular response
304 to the NPs, as observed in previous studies (Usenko et al., 2008; Klaper et al., 2009). On the
305 contrary, it is intriguing that C_{60} + B(α)P determined a significant reduction of GST activity with
306 respect to control ($p = 0.0002$) (Fig. 3C). This result agrees with previous observations concerning
307 CNPW contaminated with B(α)P (Della Torre et al., 2017). The same effect was also reported in a
308 study on zebrafish hepatocytes exposed to C_{60} and B(α)P (Ferreira et al., 2014), suggesting a
309 specific inhibition of this enzyme, which may be due to a physical interaction with the doped NPs.
310 However, the results obtained so far do not allow the identification of the mechanism underlying
311 this inhibition.

312 Concerning genotoxicity, the exposure to B(α)P alone increased significantly the DNA % in the
313 comet tail ($p < 0.0001$) as well as the LDR ($p = 0.033$) in respect to DMSO (Fig. 4F,G), but did not
314 induce cell necrosis and occurrence of MN (Fig. 4H,I). Our results confirmed the genotoxic
315 potential of B(α)P, which triggered the onset of DNA damage; its weak effect is likely related to the
316 short exposure time (72 h), which may have been not sufficient to determine fixed genetic damages,
317 as normally expected after exposure to B(α)P (Parolini et al., 2017).
318 The C_{60} administered alone did not cause any primary or fixed DNA damage compared to controls.
319 The results highlighted the absence of genotoxic effects by C_{60} in agreement with previous studies
320 showing the low genotoxic potential of C_{60} (Jacobsen et al., 2008) and the inability to generate
321 primary damage to biological systems both *in vitro* and *in vivo* (Shinoara et al., 2009; Matsuda et
322 al., 2011; Ema et al., 2012).
323 Conversely, in embryos exposed to C_{60} + B(α)P, a significantly higher frequency of necrotic cells
324 was found compared to control ($p < 0.0001$) and C_{60} administered alone ($p = 0.0012$) (Fig. 4H).
325 Exposure to C_{60} + B(α)P also resulted in the increase of MN occurrence compared to controls ($p =$
326 0.047), even if the MN frequency of this group did not exceed 5 ‰ (Fig. 4I). An extremely low
327 frequency of apoptotic cells was found in all exposure conditions (<2% data not shown). The results
328 highlighted that the adsorption of B(α)P increased the cellular damage with respect to the C_{60} alone.
329 Two possible hypotheses could explain this effect: the first one suggests that when the pollutants
330 are administered in co-exposure (C_{60} + B(α)P) they induce an increase of cell disruption without
331 direct interacting with the DNA. Alternatively, the reduction of GST activity elicited by the two
332 contaminants administered together might reduce the detoxifying capacity of the embryos, thus
333 enhancing the genotoxic effects of B(α)P. In support of the latter hypothesis, a higher cell death and
334 genotoxicity, together with the inhibition of GST activity, were observed upon exposure to CNPW
335 and C_{60} + B(α)P, in previous studies (Ferreira et al., 2014; Della Torre et al., 2017).
336
337 3.6 Functional proteomics

338 The application of proteomics allowed the identification of molecular events involved in the
339 responses to pollutants alone and in co-exposure. About 2,000 different spots in each analyzed gel
340 were visualized: 220 spots were in common between DMSO and B(α)P, 235 between control and
341 C_{60}, and 173 between control and C_{60}+B(α)P (Fig. S3). A significant variation in terms of volume
342 percentage for 28, 50 and 21 spots was measured for the three treatments, respectively. The final
343 cut-off (≥ 2-folds) revealed 23, 34 and 14 varied spots for the treatments in comparison to controls.
344 The exposure to B(α)P up-regulated 12 different proteins and down-regulated the remaining 11 with
345 respect to DMSO (Fig. S4). The C_{60} administered alone down-regulated 31 different proteins and
346 overregulated 3 of them (Fig. S4). The co-exposure C_{60} + B(α)P induced a significant over-
347 regulation of 13 proteins and down-regulation of 1 protein only (Fig. S4). Mass spectrometry
348 analysis allowed the identification of 12 changed proteins in embryos exposed to B(α)P, 27 proteins
349 for C_{60} exposure and 5 varied proteins for the co-exposure (Tab. 1,S1,S2,S3).
350 Going deeper, a variation in the amount of vitellogenin cleavage products (Vtg1,5,7) was observed
351 in all the three exposure groups. Vtgs are glycophospholipoproteins, which constitute the yolk-
352 proteins precursors in all oviparous species, including Teleosts. Vtgs are synthesized in the liver of
353 female and incorporated into oocytes where, following a proteolytic cleavage, provide essential
354 nutrients for the embryos (Byrne et al., 1989). Therefore, Vtgs proteolitic cleavage processes are
355 fundamental for the proper embryo development and the evaluation of Vtgs profiles, both at gene
356 and protein level, is considered a useful tool for highlighting toxic effects due to various types of
357 environmental pollutants (Muncke and Eggen 2006; Gundel et al., 2007; 2012; Hanish et al., 2010;
358 Ponnodurai et al., 2012; Hao et al., 2013). The C_{60}-induced down-regulation of Vtgs is in line with
359 the effects on zebrafish embryos following exposure to Quantum Dots (Petushkova et al., 2015) and
360 on adults of *Daphnia magna* exposed to Ag-NPs (Rainville et al., 2014). In this latter study, a
361 significant reduction of Vtg-like proteins was observed together with an increase in protein
362 oxidation. Therefore the down-regulation of Vtgs could be due to the protein oxidation processes as
363 a consequence of the oxidative stress generated by C_{60}.

364 In addition to nutritional function, Vtgs have a protective role towards different stressors (Sun and
365 Zhang, 2015). Particularly, the involvement of Vtg1-like proteins in the DNA repair mechanism has
366 been demonstrated in zebrafish embryos (Lai et al., 2006). Therefore, the over-regulation of Vtg1
367 observed in embryos exposed to B(α)P and to C_{60} + B(α)P might suggest the induction of a
368 protective mechanism involved, for instance, in the genotoxic damage repair processes.
369 Another protein engaged in the lipid metabolism and in metabolic processes is the
370 ApolipoproteinA-I (Apoa1b), which was modulated in embryos exposed to B(α)P and C_{60}
371 administered singly, albeit in opposite way. The alteration of Apoa1b due to modification –
372 oxidation for instance- might trigger cytotoxic and degenerative effects, therefore promoting the
373 onset of circulatory alterations (Park and Cho, 2011; Filipe et al., 2013). Indeed, a recent study
374 highlighted that the exposure of zebrafish embryos to particulate matter$_{2.5}$ ($PM_{2.5}$) could enhance the
375 occurrence of cardiovascular toxicity through the proteolitic degradation of lipoproteins (Kim et al.,
376 2015). The down-regulation of Apoa1b suggested a similar mechanism also for C_{60}. Conversely, the
377 over-regulation of Apoa1b measured in embryos exposed to B(α)P paralleled the increase of Vtg1.
378 Indeed, Apoab1 in fact also owns anti-inflammatory and antioxidant properties (Filipe et al., 2013),
379 which could contribute to the protective response of the embryos towards this pollutant.
380 The exposure to both contaminants, administered alone and in combination, affected the beta-
381 hemoglobin (BE1), a protein assigned to oxygen transport. The modulation of BE1 in fish is usually
382 related to environmental stress conditions, such as modification of temperature, salinity and
383 hypoxia (Eissa e Wang, 2016), but also to the exposure to environmental pollutants (Duarte et al.,
384 2010; Narra 2016). The observed alteration of BE1 content might affect oxygen supply, thereby
385 compromising the development and survival of the embryos.
386 The exposure to C_{60} induced the down-regulation of several kinases such as muscle creatine kinase
387 A (Ckma), creatine kinase M-type isoform X1 (Ckmb) and nucleoside diphosphate kinase B
388 (Nme2b.2). These proteins are involved in cellular signaling, growth and differentiation, as well as
389 energetic metabolism (Tanimura et al., 2014). The alteration of kinases levels might induce the

onset of negative effects on embryos. Indeed, the loss of Nme2b.2 induced severe vasculature malformations (Feng et al., 2014) and cardiomyopathy (Hippe et al., 2009) in zebrafish embryos.

The exposure to B(α)P determined a down-regulation of Type I cytokeratin enveloping layer (Cyt1). Cytokeratins are structural proteins involved in the formation of intermediate filaments of epithelial cells and in the mainteinance of cell integrity and adhesion in tissues, promoting resistance to mechanical stress (Padhi et al., 2006). The down-regulation of several keratins (Krt4, Krt5 e Krt8) has been already observed in zebrafish embryos exposed to B(α)P (20 μg/L) (Binelli et al., 2017), supporting the hypothesis that this chemical is able to affect the functionality of structural proteins.

Another down-regulated protein in embryos exposed to B(α)P is the Fatty Acid Binding Protein7 (Fabp7), a chaperonine responsible for cellular fatty acid transport (Furuhashi and Hotamisligil, 2013). At the embryonic level, Fabp7 plays a key role in the development of the central nervous system and affects proper development of the visual system (Liu et al., 2004). Therefore, B(α)P might alter the development and function of the nervous system and the visual apparatus through the down-regulation of Fabp7, as previously suggested (He et al., 2012; Binelli et al., 2017).

Overall, proteomic analysis confirmed the different mechanism of action of single contaminants and their combination. Results suggested that the oxidative stress generated by C_{60} triggers a general reduction of the metabolic activity in the embryos, confirming recent findings of Lv and coauthors (2017), who suggested that the toxicity of C_{60} in *D. magna* might be correlated with oxidative stress and reduction of energy acquisition. On the contrary, B(α)P alone and adsorbed on C_{60} up-regulated proteins involved in the homeostatic response to cellular stress.

4. Conclusions

The present study showed how the adsorption of B(α)P by C_{60} altered the hydrodynamic behavior of the NPs, consequently reducing their bioavailability and intake by the embryos. We showed that

the B(α)P adsorbed on C_{60} is bioavailable and accumulated in embryos. The integration of data obtained through biomarkers and functional proteomics suggests that B(α)P alone and C_{60} + B(α)P affect similar cellular mechanisms, with the latter triggering severer cellular damages.

Our results highlight that, in the natural environment complex chemico-physical-biological interactions arise, possibly determining unexpected ecotoxicological consequences for the organisms.

Acknowledgements

This study was financially supported by the "Cariplo Foundation" grant number 2013-0817. We are grateful to Giorgio Binelli for his precious advices on statistical analysis.

Figure Captions

Figure 1 C_{60} characterization. DLS profile of C_{60} alone and contaminated with B(α)P, in zebrafish water (A). Particle size distribution of 3 measurements of 10 runs is given by numbers. UV-Vis spectra of C_{60} suspensions (B).

Figure 2. **C_{60} observation in embryos**. TEM images showing C_{60} indicated by arrows in gut (A) of embryos exposed to C_{60} and in gut (B) and gills (C) of C_{60} + B(α)P. n = nucleus, m = mitochondrion, mv = microvilli, l = lumen.

Figure 3. **B(α)P accumulation**. Cryostate sections showing the uptake of B(α)P (in red) in gills (C,D,E) and digestive apparatus (F,G,H) of zebrafish embryos. Controls (A-B), B(α)P (C,F), C_{60} + B(α)P (D-G) and C_{60} (E,H). DNA (nuclei) is marked in blue (DAPI coloration). SB = swim bladder, L = gut lumen, Y = yolk sac.

Figure 4. Effects on biomarkers. Effects on the activity (mean ± SEM) of SOD (A) CAT (B), GST (C); protein carbonylation (D); and genotoxic effects as DNA strand breaks (E), LDRs (F), occurrence of necrotic cells (G) and MN (H) measured in zebrafish embryos (96 hpf) (*n* = 3; pool of

439 3 independent experiments). Different letters correspond to values significantly different (one-way
440 ANOVA, Duncan's *post-hoc* test, $p < 0.05$).
441
442
443 **References**

444 1. Al-Subiai, S.N., Arlt, V.M., Frickers, P.E., Readman, J.W., Stolpe, B., Lead, J.R., Moody, A.J., Jha,
445 A.N., 2012. Merging nano-genotoxicology with eco-genotoxicology: an integrated approach to
446 determine interactive genotoxic and sub-lethal toxic effects of C(60) fullerenes and fluoranthene in
447 marine mussels, *Mytilus sp*., Mutat. Res. 745*,* 92-103.
448 2. Astefanei, A., Núnez, O., Galceran, M.T., 2014. Analysis of C60-fullerene derivatives and pristine
449 fullerenes in environmental samples by ultrahigh performance liquid chromatography–atmospheric
450 pressure photoionization-mass spectrometry, J. Chromatogr. A 1365, 61–71.
451 3. Baun, A., Sorensen, S.N., Rasmussen, R.F., Hartmann, N.B., Koch, C.B., 2008. Toxicity and
452 bioaccumulation of xenobiotic organic compounds in the presence of aqueous suspensions of
453 aggregates of nano-C-60. Aquat. Toxicol. 86, 379−387.
454 *4.* Binelli, A., Del Giacco, L., Santo, N., Bini, L., Magni, S., Parolini, M., Madaschi, L., Ghilardi, A.,
455 Maggioni, D., Ascagni, M., Armini, A., Prosperi, L., Landi, C., La Porta, C., Della Torre, C., 2017.
456 Carbon Nanopowder act as a Trojan-horse for Benzo(a)pyrene in *Danio rerio* embryos.
457 Nanotoxicology 11, 371-381.
458 5. Byrne, B.M., Gruber, M., Gruber, A.B., 1989. The evolution of yolk proteins. Progr. Biophys Mol.
459 Biol. 53, 33–69.
460 6. Carboni, A., Helmus, R., Parsons, J.R., Kalbitz, K., de Voogt, P., 2016. A method for the
461 determination of fullerenes in soil and sediment matrices using ultra-high performance liquid
462 chromatography coupled with heated electrospray quadrupole time of flight mass spectrometry. J.
463 Chromatogr. A 1433, 123–130.
464 7. Canesi, L., Fabbri, R., Gallo, G., Vallotto, D., Marcomini, A., Pojana, G., 2010. Biomarkers in
465 Mytilus galloprovincialis exposed to suspensions of selected nanoparticles (Nano carbon black, C60
466 fullerene, Nano-TiO_2, Nano-SiO_2). Aquat. Toxicol. 100, 168-177.

8. Chen, Q., Yin, D., Li, J., Hu, X., 2014. The effects of humic acid on the uptake and depuration of fullerene aqueous suspensions in two aquatic organisms. Environ. Toxicol. Chem. 33, 1090-1097.
9. Della Torre, C., Parolini, M., Del Giacco, L., Ghilardi, A., Ascagni, M., Santo, N., Maggioni, D., Magni, S., Madaschi, L., Prosperi, L., La Porta, C., Binelli, A., 2017. Adsorption of B(α)P on Carbon Nanopowder affects accumulation and toxicity on zebrafish (*Danio rerio*) embryos. Environ. Sci: Nano 4, 1132-1146.
10. Driessen, M.D., Mues, S., Vennemann, A., Hellack, B., Bannuscher, A., Vimalakanthan, V., Riebeling, C., Ossig, R., Wiemann, M., Schnekenburger, J., Kuhlbusch, T.A.J., Renard, B., Luch, A., Haase, A., 2015. Proteomic analysis of protein carbonylation: a useful tool to unravel nanoparticle toxicity mechanisms. Part. Fibr. Toxicol. 12,36.
11. Duarte, R.M., Honda, R.M., Val, A.L., 2010. Acute effects of chemically dispersed crude oil on gill ion regulation, plasma ion levels and haematological parameters in tambaqui (*Colossoma macropomum*). Aquat. Toxicol. 97, 134-141.
12. Eissa, N., Wang, H-P., 2016. Transcriptional stress responses to environmental and husbandry stressors in aquaculture species. Rev. Aquacult. 8, 61–88.
13. Ema, M., Tanaka, J., Kobayashi, N., Naya, M., Endoh, S., Maru, J., Hosoi, M., Nagai, M., Nakajima, M., Hayashi, M., Nakanishi, J., 2012. Genotoxicity evaluation of fullerene C_{60} nanoparticles in a comet assay using lung cells of intratracheally instilled rats. Regulat. Toxicol. Pharmacol. 62, 419–424.
14. Fan, W., Peng, P., Li, X., Ren, J., Liu, T., Wang, X., 2016. Effect of titanium dioxide nanoparticles on copper toxicity to *Daphnia magna* in water: Role of organic matter. Water Res. 105, 129-137.
15. Farre, M., Perez, S., Gajda-Schrantz, K., Osorio, V., Kantiani, L., Ginebreda, A., Barceló, D., 2010. First determination of C_{60} and C_{70} fullerenes and N- methylfullereopyrrolidine C_{60} on the suspended material of wastewater effluents by liquid chromatography hybrid quadrupole linear ion trap tandem mass spectrometry. J. Hydrol. 383, 44–51.
16. Ferreira, J.L., Lonne, M.N., França, T.A., Maximilla, N.R., Lugokenski, T.H., Costa, P.G., Fillmann, G., Soares, F.A., de la Torre, F.R., Monserrat, J.M., 2014. Co-exposure of the organic nanomaterial fullerene C_{60} with benzo[a]pyrene in *Danio rerio* (zebrafish) hepatocytes: evidence of toxicological

interactions. Aquat. Toxicol. 147, 76-83.

17. Feng, Y., Gross, S., Wolf, N.M., Butenschön, V.M., Qiu, Y., Devraj, K., Liebner, S., Kroll, J., Skolnik, E.Y., Hammes, H-P., Wieland, T., 2014. Nucleoside Diphosphate Kinase B Regulates Angiogenesis Through Modulation of Vascular Endothelial Growth Factor Receptor Type 2 and Endothelial Adherens Junction Proteins. Arterioscler. Thromb. Vasc. Biol. 34, 2292-2300.
18. Filipe, P., Morlière, P., Silva, J.N., Mazière, J-C., Patterson, L.K., Freitas, J.P., Santus, R., 2013. Plasma Lipoproteins as Mediators of the Oxidative Stress Induced by UV Light in Human Skin: A Review of Biochemical and Biophysical Studies on Mechanisms of Apolipoprotein Alteration, Lipid Peroxidation, and Associated Skin Cell Responses. Ox. Med. Cell. Longev. 285825.
19. Freitas Cordeiro, L., Marques, B.F., Wilges Kist, L., Bogo, M.R., Lopez, G., Pagano, G., Clemes I., Guerreiro, K., Monserrat, J.M., 2014. Toxicity of fullerene and nanosilver nanomaterials against bacteria associated to the body surface of the estuarine worm *Laeonereis acuta* (Polychaeta, Nereididae). Mar. Environ. Res. 99, 52-59.
20. Furuhashi, M., Hotamisligil, G.S., 2008. Fatty acid-binding proteins: role in metabolic diseases and potential as drug targets. Nat. Rev. 7, 489-503.
21. Gorrochategui, E., Li, J., Fullwood, N.J., Ying, G-G., Tian, M., Cui, L., Shen, H., Lacorte, S., Tauler, R., Martin, F.L., 2017. Diet-sourced carbon-based nanoparticles induce lipid alterations in tissues of zebrafish (*Danio rerio*) with genomic hypermethylation changes in brain. Mutagenesis 32, 91–103.
22. Gündel, U., Benndorf, D., von Bergen, M., Altenburger, R., Küster, E., 2007. Vitellogenin cleavage products as indicators for toxic stress in zebra fish embryos: A proteomic approach. Proteomics 7, 4541–4554.
23. Gündel, U., Kalkhof, S., Zitzkat, D., von Bergen, M., Altenburger, R., Küster, E., 2012. Concentration–response concept in ecotoxicoproteomics: Effects of different phenanthrene concentrations to the zebrafish (*Danio rerio*) embryo proteome. Ecotoxicol. Environ. Saf. 76, 11-22.
24. Hanisch, K., Kuster, E., Altenburger, R., Gundel, U., 2010, Proteomic Signatures of the Zebrafish (Danio rerio) Embryo: Sensitivity and Specificity in Toxicity Assessment of Chemicals. Int. J. Proteom.. 630134.

25. Hao, R., Bondesson, W., Singh, A.V., Riu, A., McCollum, C.W., Knudsen, T.B., Gorelick, D.A., Gustafsson, J-A., 2013. Identification of Estrogen Target Genes during Zebrafish Embryonic Development through Transcriptomic Analysis. PlosOne 11, e79020.

26. He, C., Wang, C., Zhou, Y., Li, J., Zuo, Z., 2012. Embryonic exposure to benzo(a)pyrene influences neural development and function in rockfish (*Sebastiscus marmoratus*). Neurotoxicology 33, 758-762.

27. Henry, T.B., Wileman, S.J., Boran, H., Sutton, P., 2013. Association of Hg2+ with aqueous (C60)n aggregates facilitates increased bioavailability of Hg2+ in zebrafish (*Danio rerio*). Environ. Sci. Technol. 47, 9997-10004.

28. Hippe, H-J., Wolf, N.M., Abu-Taha, I., Mehringer, R., Just, S., Lutz, S., Niroomand, F., Postel, E.H., Katus, H.A., Rottbauer, W., Wieland, T., 2009. The interaction of nucleoside diphosphate kinase B with G dimers controls heterotrimeric G protein function. Proceed. Nat. Am. Soc. 106, 16269-16274.

29. Hu, X., Li, J., Chen, Q., Lin, Z., Yin, D., 2014. Combined effects of aqueous suspensions of fullerene and humic acid on the availability of polycyclic aromatic hydrocarbons: Evaluated with negligible depletion solid-phase microextraction. Sci. Tot. Environ. 493, 12-21.

30. Huffer, T., Sun, H., Kubicki, J.D., Hofmann, T., Kah, M., 2017. Interactions between aromatic hydrocarbons and functionalized C_{60} fullerenes – insights from experimental data and molecular modelling. Environ. Sci: Nano 4, 1045-1052.

31. Jacobsen, N.R., Pojana, G., White, P., Muller, P., Cohn, C.A., Korsholm, K.S., Vogel, U., Marcomini,A., Loft, S., Wallin, H., 2008. Genotoxicity, Cytotoxicity, and Reactive Oxygen Species Induced by Single-Walled Carbon Nanotubes and C_{60} Fullerenes in the FE1-Muta™ Mouse Lung Epithelial Cells. Environ. Mol. Mutagen. 49, 476-487.

32. Kim, J-Y., Lee, E-Y., Inho Choi, I., Kim, J., Cho, K-H., 2015. Effects of the Particulate Matter$_{2.5}$ ($PM_{2.5}$) on Lipoprotein Metabolism, Uptake and Degradation, and Embryo Toxicity. Mol. Cells 38, 1096-1104.

33. Klaper, R., Crago, J., Barr, J., Arndt, D., Setyowati, K., Chen, J., 2009. Toxicity biomarker expression in daphnids exposed to manufactured nanoparticles: Changes in toxicity with functionalization. Environ. Pollut. 157l, 1152-1156.

551 34. Lai, Y-S., Chiue, L-F., Hsu, T., 2006. Low-Molecular-Weight Vitellogenin 1-Like Proteins are
552 Components of a UV-Damaged-DNA Binding Activity Highly Expressed in Zebrafish (*Danio*
553 *rerio*) Embryos. J. Exp. Zool. 305A, 215–224.
554 35. Li, J., Hu, L-X., Ying, G-G., Martin, F.L, 2017. Co-exposure of C_{60} fullerene with benzo[a]pyrene
555 results in enhanced biological effects in cells as determined by Fourier-transform infrared
556 spectroscopy. Environ. Sci: Nano 4, 1404-1418.
557 36. Liu, R.Z., Denovan-Wright, E.M., Degrave, A., Thisse, C., Thisse, B., Wright, J.M., 2004.
558 Differential expression of duplicated genes for brain-type fatty acid-binding proteins (fabp7a and
559 fabp7b) during early development of the CNS in zebrafish (*Danio rerio*). Gen. Express. Patt. 4,
560 379–387.
561 37. Lu, J., Nagase, S., Zhang, X., Wang, D., Ni, M., Maeda, Y., Wakahara, T., Nakahodo, T., Tsuchiya,
562 T., Akasaka, T., Gao, Z., Yu, D., Ye, H., Mei, W.N., Zhou, Y., 2006. Selective Interaction of Large
563 or Charge-Transfer Aromatic Melecules with Metallic Single-Wall Carbon Nanotubes: Critical Role
564 of the Molecular Size and Orientation. J. Am. Chem. Soc. 128, 5114–5118.
565 38. Lv X., Huang, B., Zhu, X., Jiang, Y., Chen, B., Tao, Y., Zhou, J., Cai, Z., 2017. Mechanisms
566 underlying the acute toxicity of fullerene tu Daphnia magna: Energy acquisition restriction and
567 oxidative stress. Wat. Res. 123, 696-703.
568 39. Matsuda, S., Matsui, S., Shimizu, Y., Matsuda, T., 2011. Genotoxicity of Colloidal Fullerene C60.
569 Environ. Sci. Technol. 45, 4133–4138.
570 40. Mousavi, S.Z., Nafisi, S., Maibach, H.I., 2017. Fullerene nanoparticle in dermatological and
571 cosmetic applications. Nanomed: Nanotechnol. Biol. Med. 13, 1071–1087.
572 41. Muncke, J., Eggen, R.I.L., 2006. Vitellogenin 1 mRNA as an early molecular biomarker for
573 endocrine disruption in developing zebrafish (*Danio rerio*). Environ. Toxicol. Chem. 25, 2734–41.
574
575 42. Narra, M.R., 2016. Single and cartel effect of pesticides on biochemical and haematological status of
576 *Clarias batrachus*: A long-term monitoring. Chemosphere 144, 966-974.
577 43. Padhi, B.K., Akimenko, M-A., Ekker, M., 2006. Independent expansion of the keratin gene family in
578 teleostean fish and mammals: An insight from phylogenetic analysis and radiation hybrid mapping

of keratin genes in zebrafish. Gene 368, 37–45.

44. Papaconstantinou, J., 2009. Oxidative modification and aggregation of creatine kinase from aged mouse skeletal muscle. Aging 1, 557-572.

45. Park, K-H., Cho, K-H., 2011. A zebrafish model for the rapid evaluation of pro-oxidative and inflammatory death by lipopolysaccharide, oxidized low-density lipoproteins, and glycated high-density lipoproteins. Fish Shell. Immunol. 31, 904-910.

46. Park, J.W., Henry, T. B., Ard, S., Menn, F. M., Compton, R. N., Sayler, G. S., 2011. The association between nC(60) and 17 alpha- ethinylestradiol (EE2) decreases EE2 bioavailability in zebrafish and alters nanoaggregate characteristics. Nanotoxicology 5, 406−416.

47. Parolini, M., Ghilardi, A., Della Torre, C., Magni, S., Prosperi, L., Calvagno, M., Del Giacco, L., Binelli, A., 2017. Environmental concentrations of cocaine and its main metabolites modulated antioxidant response and caused cyto-genotoxic effects in zebrafish embryo cells. Environ. Pollut. 226, 504-514.

48. Pavagadhi, S., Sathishkumar, M., Balasubramanian, R., 2014. Uptake of Ag and TiO2 nanoparticles by zebrafish embryos in the presence of other contaminants in the aquatic environment. Wat. Res. 55, 280-291.

49. Petushkova, N.A., Kuznetsova, G.P., Larina, O.V., Kisrieva, Y.S., Samenkova, N.F., Trifonova, O.P., Miroshnichenko, Y.V., Zolotarev, K.V., Karuzina, I.I., Ipatova O.M., Lisitsa A.V., 2015. One-dimensional proteomic profiling of *Danio rerio* embryo vitellogenin to estimate quantum dot toxicity. Proteom. Sci. 13, 17.

50. Ponnudurai RP, Basak T, Ahmad S, Bhardwaj G, Chauhan RK, Singh RA, et al. 2012. Proteomic analysis of zebrafish (*Danio rerio*) embryos exposed to cyclosporine A. J. Prot. 75, 1004–17. □

51. Rainville, L-C., Carolan, D., Varela, A.C., Doyle, H., Sheehan, D., 2014. Proteomic evaluation of citrate-coated silver nanoparticles toxicity in *Daphnia magna.* Analyst 139, 1678-1686.

52. Sanchis, J., Berrojalbiz, N., Caballero, G., Dachs, J., Farre, M., Barcelo, D., 2012. Occurrence of aerosol-bound fullerenes in the mediterranean sea atmosphere. Environ. Sci. Technol. 46, 1335–1343. □

53. Sanchis, J., Oliviera, L.F., Leão, F.B., Farre, M., Barcelo, D., 2015. Liquid chromatography–

atmospheric pressure photoionization–Orbitrap analysis of fullerene aggregates on surface soils and river sediments from Santa Catarina (Brazil). Sci. Tot. Eniron. 505, 172–179. □

54. Seke, M., Milica Markelic, M., Morina, A., Jovic, D., Korac, A., Milicic, D., Djordjevic, A., 2017. Synergistic mitotoxicity of chloromethanes and fullerene C_{60} nanoaggregates in *Daphnia magna* midgut epithelial cells. Protoplasma 254, 1607-1616.
55. Shinohara, N., Matsumoto, K., Endoh, S., Maru, J., Nakanishi, J., 2009. *In vitro* and *in vivo* genotoxicity tests on fullerene C_{60} nanoparticles. Toxicol. Lett. 191, 289-296.
56. Su, Y., Yan, X.M., Pu, Y.B., Xiao, F., Wang, D.S., Yang, M., 2013. Risks of Single-Walled Carbon Nanotubes Acting as Contaminants- Carriers: Potential Release of Phenanthrene in Japanese Medaka (Oryzias latipes). Environmen. Sci. Technol. 47, 4704−4710.
57. Sun, C., Zhang S., 2015. Immune-Relevant and Antioxidant Activities of Vitellogenin and Yolk Proteins in Fish. Nutrients 7, 8818–8829.
58. Tanimura, A., Horiguchi, T., Miyoshi, K., Hagita, H., Noma, T., 2014. Differential Expression of Adenine Nucleotide Converting Enzymes in Mitochondrial Intermembrane Space: A Potential Role of Adenylate Kinase Isozyme 2 in Neutrophil Differentiation. PlosOne 9, e89916.
59. Usenko, C.Y., Harper, S.L., Tanguay, R.L., 2008. Fullerene C_{60} exposure elicits an oxidative stress response in embryonic zebrafish. Toxicol. Appl. Pharmacol. 229, 44–55.
60. van der Oost, R., Beyer, J., Vermeulen, N.P.E., 2003. Fish bioaccumulation and biomarkers in environmental risk assessment: a review. Environ. Toxicol. Pharmacol. 13, 57–149.
61. van der Ploeg, M.J.C., Baveco, J.M., van der Hout, A., Bakker, R., Rietjens, I.M.C.M., van den Brink, N.W., 2011. Effects of C60 nanoparticle exposure on earthworms (Lumbricus ruellus) and implications for population dynamics. Environmen. Pollut. 159, 198–203.
62. Velzeboer, I., Kwadijk, C.J.A.F., Koelmans, A.A., 2014. Strong Sorption of PCBs to Nanoplastics, Microplastics, Carbon Nanotubes, and Fullerenes. Environ. Sci. Technol. 48, 4869-4876.
63. Waissi, G.C., Bold, S., Pakarinen, K., Akkanen, J., Leppänen, M.T., Petersen, E.J., Kukkonen, J.V.K., 2017. *Chironomus riparius* exposure to fullerene-contaminated sediment results in oxidative stress and may impact life cycle parameters. J. Haz. Mat. 322, 301-309.
64. Wang, Z., Zhao, J., Song, L., Mashayekhi, H., Chefetz, B., Xing. B., 2011. Adsorption and

635 Desorption of Phenanthrene on Carbon Nanotubes in Simulated Gastrointestinal Fluids. Environ.
636 Sci. Technol. 45, 6018-6024.
637 65. Yadav, B.C., Kumar, R., 2008. Structure, properties and applications of fullerenes. Int. J.
638 Nanotechnol. Applicat. 2, 15-24.
639 66. Yang, K., Zhu, L.Z., Xing, B.S., 2006. Adsorption of polycyclic aromatic hydrocarbons by carbon
640 nanomaterials. Environ. Sci. Technol. 40, 1855–1861.
641 67. Yang, X.Y., Edelmann, R.E., Oris, J.T., 2010. Suspended C60 nanoparticles protect against short-
642 term UV and fluoranthene photo-induced toxicity, but cause long-term cellular damage in *Daphnia*
643 *magna*. Aquat. Toxicol. 100, 202-210.
644
645

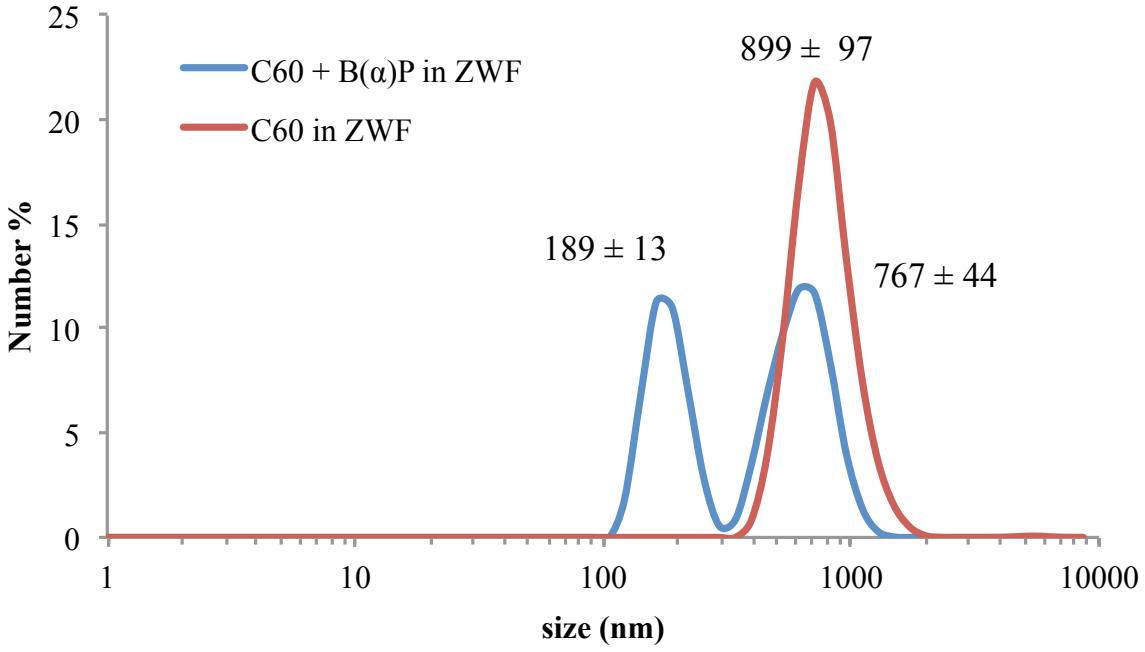
25
20
15
10
5
0
Number %
C60 + B(α)P in ZWF
C60 in ZWF
899 ± 97
189 ± 13
767 ± 44
1
10
100
1000
10000
size (nm)

A

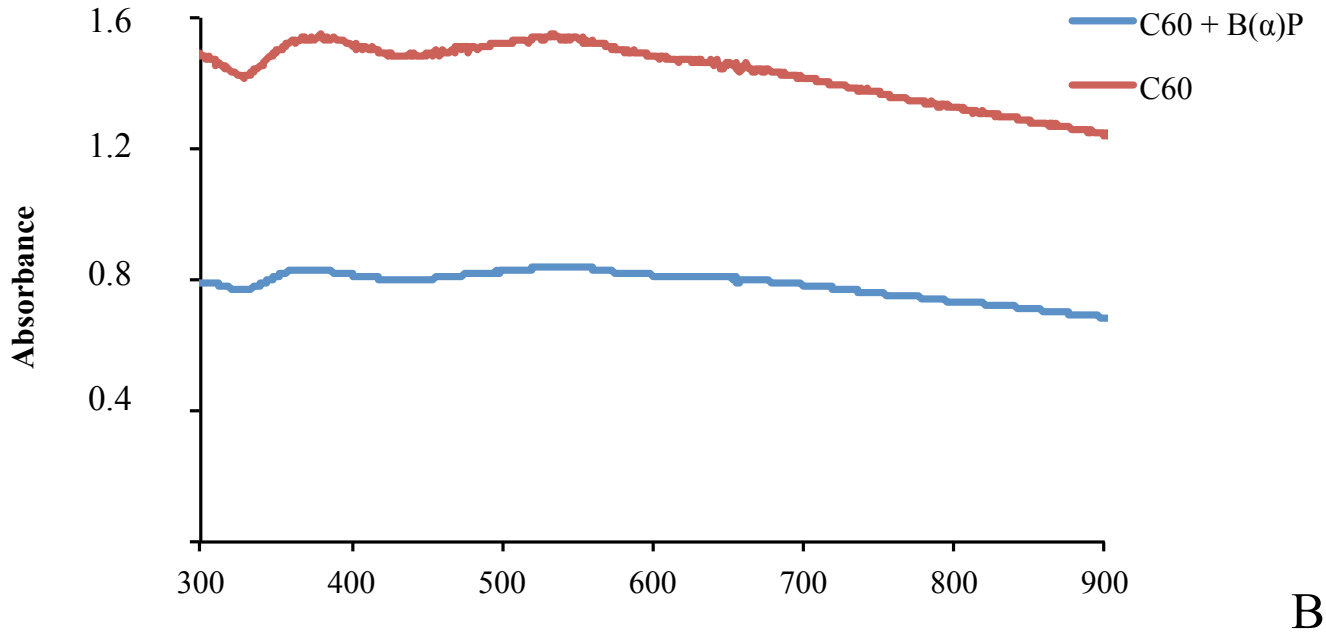
1.6
1.2
0.8
0.4
Absorbance
C60 + B(α)P
C60
300
400
500
600
700
800
900

B

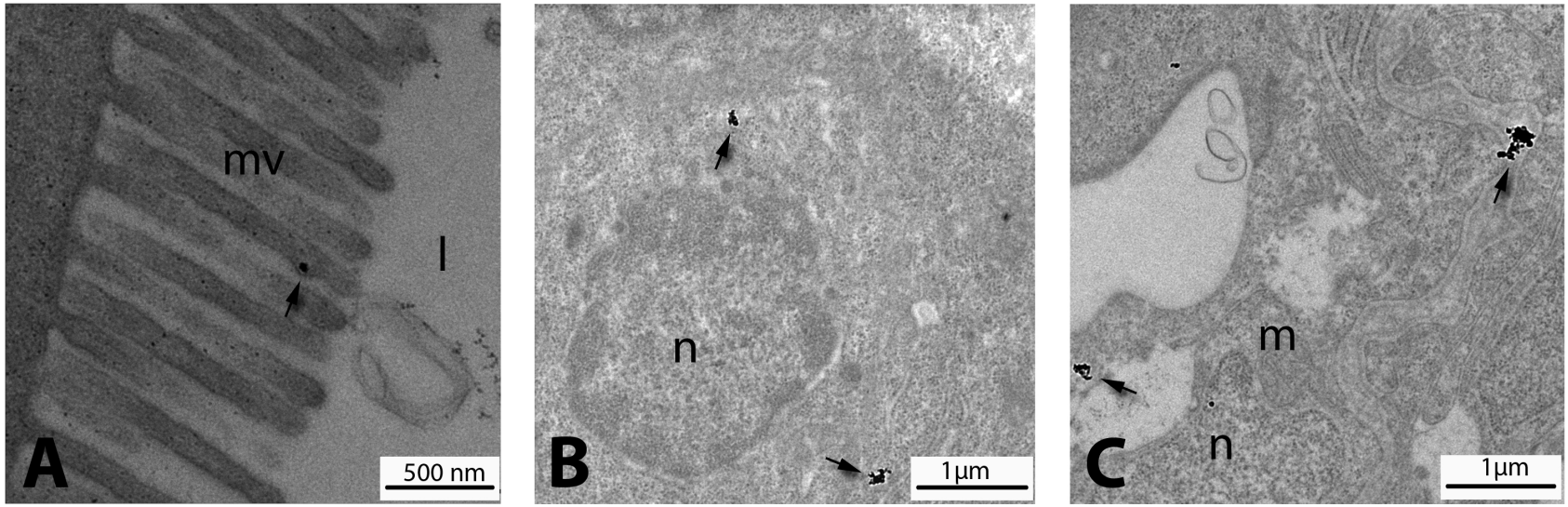
mv
l
A
500 nm
n
B
1µm
m
n
C
1µm

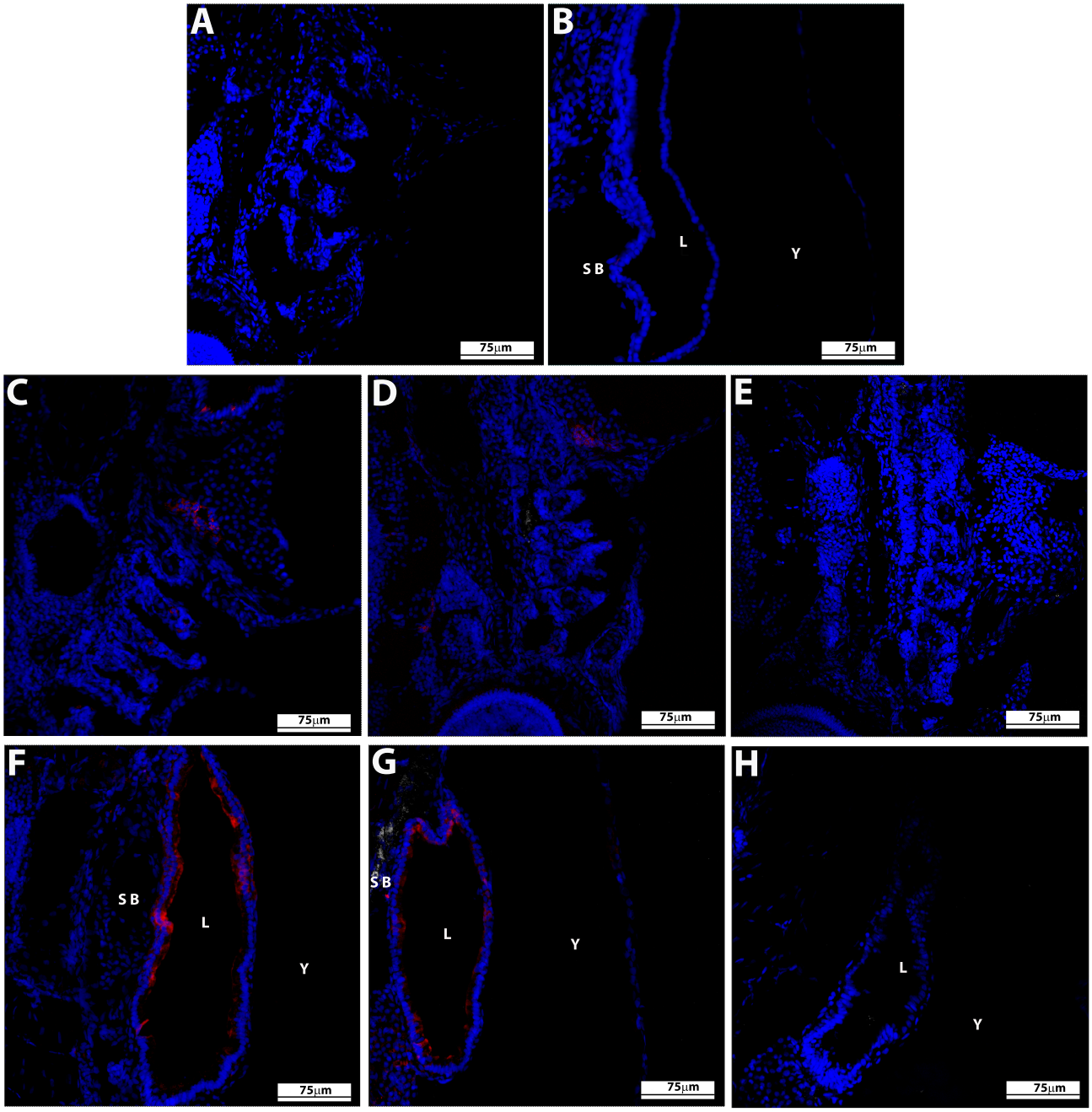
A
B
SB
L
Y
75µm
C
D
E
F
G
H

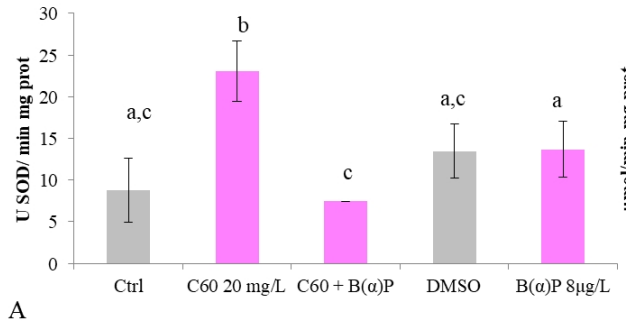
U SOD/ min mg prot
30
25
20
15
10
5
0
a,c
b
c
a,c
a
Ctrl
C60 20 mg/L
C60 + B(α)P
DMSO
B(α)P 8µg/L

A

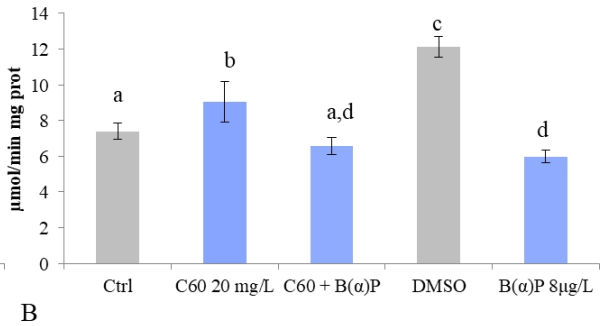
µmol/min mg prot
14
12
10
8
6
4
2
0
a
b
a,d
c
d
Ctrl
C60 20 mg/L
C60 + B(α)P
DMSO
B(α)P 8µg/L

B

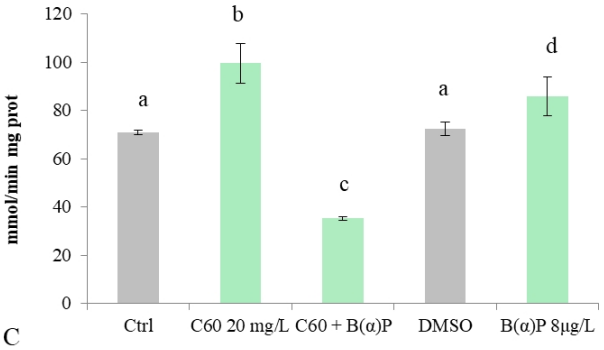
mmol/min mg prot
120
100
80
60
40
20
0
a
b
c
a
d
Ctrl
C60 20 mg/L
C60 + B(α)P
DMSO
B(α)P 8µg/L

C

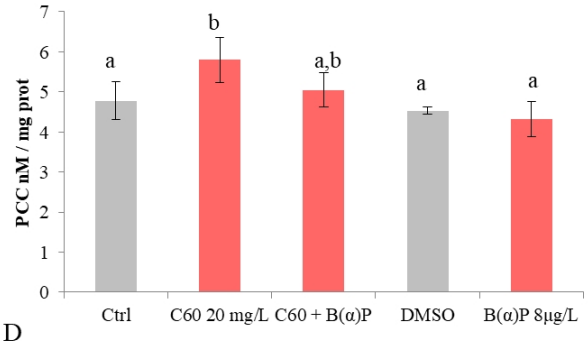
PCC nM / mg prot
7
6
5
4
3
2
1
0
a
b
a,b
a
a
Ctrl
C60 20 mg/L
C60 + B(α)P
DMSO
B(α)P 8µg/L

D

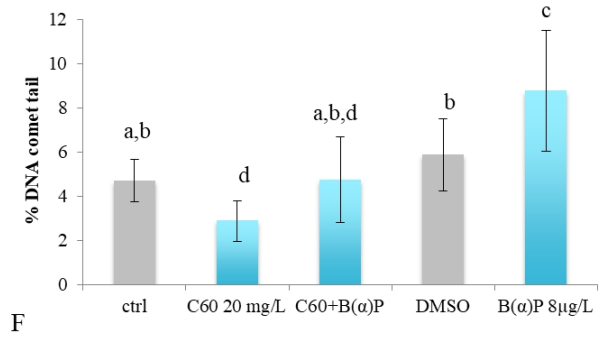
% DNA comet tail
12
10
8
6
4
2
0
a,b
d
a,b,d
b
c
ctrl
C60 20 mg/L
C60+B(α)P
DMSO
B(α)P 8µg/L

F

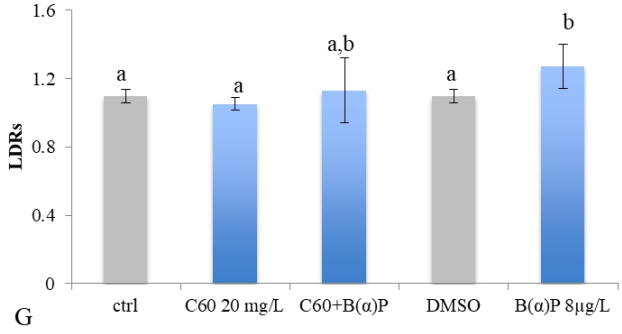
LDRs
1.6
1.2
0.8
0.4
0
a
a
a,b
a
b
ctrl
C60 20 mg/L
C60+B(α)P
DMSO
B(α)P 8µg/L

G

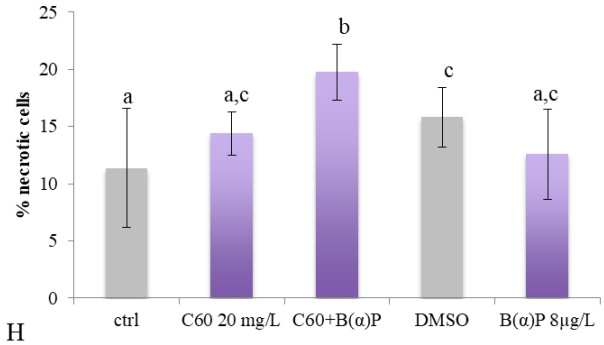
% necrotic cells
25
20
15
10
5
0
a
a,c
b
c
a,c
ctrl
C60 20 mg/L
C60+B(α)P
DMSO
B(α)P 8µg/L

H

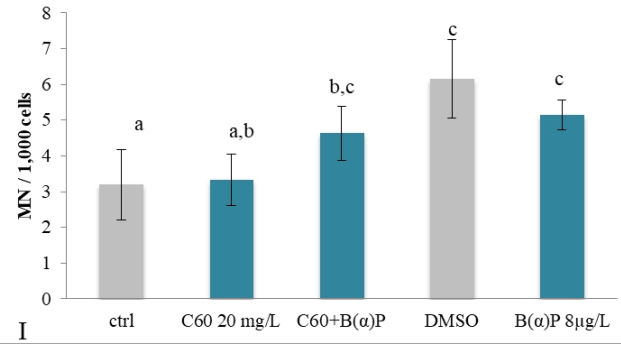
MN / 1,000 cells
8
7
6
5
4
3
2
1
0
a
a,b
b,c
c
c
ctrl
C60 20 mg/L
C60+B(α)P
DMSO
B(α)P 8µg/L

I

Table1 Proteins modified in zebrafish embryos upon exposure to C_{60} and B(α)P singly and in combination

Spot[a]	Fold change (↓/↑)[b]	Protein identification	NCBInr Accession number	Molecular function[c]
B(α)P vs DMSO				
2	2.3↓	Type I cytokeratin. enveloping layer (Cyt1)	AAH65653.1	Structural molecule activity
6	3.2↑	Apolipoprotein A-I precursor (Apoa1b)	NP_001093614.2	Lipid transport
7	3.6↑	Hemoglobin beta embryonic-1.1 (BE1)	NP_932339.1	Oxygen transport
9	2.5↑	Hemoglobin beta embryonic-1.1 (BE1)	NP_932339.1	Oxygen transport
11	2.0↓	Fatty acid binding protein 7, brain, a (Fabp7a)	NP_571680.1	Lipid transport
14	2.9↑	Vitellogenin 1 (Vtg 1)	AAH94995.1	Lipid transport
19	2.8↑	Hemoglobin beta embryonic-1.1 (BE1)	NP_932339.1	Oxygen transport
20	2.5↑	Vitellogenin 1 (Vtg 1)	AAH94995.1	Lipid transport
21	2.5↑	Hemoglobin beta embryonic-1.1 (BE1)	NP_932339.1	Oxygen transport
27	3.6↑	Vitellogenin 1 (Vtg 1)	AAH94995.1	Lipid transport
30	2.0↓	Vitellogenin 5 (Vtg 5)	AAH97081.1	Lipid transport
C_{60} vs Ctrl				
1	4.0↓	Vitellogenin 1 (Vtg 1)	AAH94995.1	Lipid transport
5	3.5↓	Vitellogenin 1 (Vtg 1)	AAH94995.1	Lipid transport
6	2.9↓	Vitellogenin 1 (Vtg 1)	AAH94995.1	Lipid transport
7	3.0↓	muscle creatine kinase a (Ckma)	NP_571007.2	Kinase activity ATP binding
9	3.4↓	Vitellogenin 1 (Vtg 1)	AAH94995.1	Lipid transport
10	2.1↓	Vitellogenin 1 (Vtg 1)	AAH94995.1	Lipid transport
11	2.0↓	Apolipoprotein A-I precursor (Apoa1b)	NP_001093614.2	Lipid transport
12	3.0↓	Vitellogenin 1 (Vtg 1)	AAK94945.1	Lipid transport
13	2.3↓	Vitellogenin 1 precursor (Vtg 1)	NP_001038362.3	Lipid transport
16	3.7↓	Vitellogenin 1 (Vtg 1)	AAI39514.1	Lipid transport
17	2.7↓	Hemoglobin beta embryonic-1.1 (BE1)	NP_932339.1	Oxygen transport
20	3.2↓	Hemoglobin beta embryonic-1.1 (BE1)	NP_932339.1	Oxygen transport
21	3.2↓	Vitellogenin 1 (Vtg 1)	AAK94945.1	Lipid transport
22	8.1↓	Vitellogenin 1 (Vtg 1)	AAH94995.1	Lipid transport
24	7.2↓	Vitellogenin 7 (Vtg7)	AAW56971.1	Lipid transport
26	2.8↓	muscle-specific creatine kinase (Ckma)	AAK64515.1	Kinase activity ATP binding
27	2.8↓	muscle-specific creatine kinase (Ckma)	AAK64515.1	Kinase activity ATP binding
32	3.1↓	Vitellogenin 1 (Vtg 1)	AAH94995.1	Lipid transport
33	4.9↓	Hemoglobin beta embryonic-1.1 (BE1)	NP_932339.1	Oxygen transport
35	2.6↓	Vitellogenin 1 (Vtg 1)	AAH94995.1	Lipid transport
38	3.0↓	creatine kinase M-type isoform X1 (Ckmb)	XP_005157650.1	Kinase activity ATP binding
43	3.0↓	nucleoside diphosphate kinase B (Nme2b.2)	NP_571002.1	ATP binding
46	2.3↓	Vitellogenin 1 (Vtg 1)	AAK94945.1	Lipid transport
47	3.3↓	Hemoglobin beta embryonic-1.1 (BE1)	NP_932339.1	Oxygen transport
52	2.3↓	Vitellogenin 1 precursor (Vtg 1)	NP_001038362.3	Lipid transport
53	2.7↓	nucleoside diphosphate kinase B (Nme2b.2)	NP_571002.1	ATP binding
54	3.0↓	Vitellogenin 1 (Vtg 1)	AAK94945.1	Lipid transport
C_{60} + B(α)P vs Ctrl				
1	4.1↑	Vitellogenin 1 (Vtg 1)	AAH94995.1	Lipid transport
5	4.1↑	Vitellogenin 1 (Vtg 1)	AAI39514.1	Lipid transport
7	2.9↑	Vitellogenin 1 (Vtg 1)	AAI39514.1	Lipid transport
8	2.4↑	Hemoglobin beta embryonic-1.1 (BE1)	NP_932339.1	Oxygen transport
12	2.8↑	Vitellogenin 1 (Vtg 1)	AAH94995.1	Lipid transport

[a] ID number of spot on 2-DE map;

[b] fold change increase (↑) or decrease (↓) in terms of relative spot volume (%V) in comparison with control (ZFW or DMSO);

[c] from www.uniprot.org site.

Supporting information

The interactions of Fullerene C_{60} and Benzo(α)pyrene influence their bioavailability and toxicity to zebrafish embryos

Camilla Della Torre, Daniela Maggioni, Anna Ghilardi, Marco Parolini, Nadia Santo, Claudia Landi, Laura Madaschi, Stefano Magni, Stefano Tasselli, Miriam Ascagni, Luca Bini, Caterina La Porta, Luca Del Giacco, Andrea Binelli

1. Methods

1.1 Fluorescence detection of B(α)P adsorption on C_{60}

Excitation and emission spectra were obtained with an Edinburgh FLS980 spectrofluorometer equipped with a 450 W xenon arc lamp. The spectra were corrected for source intensity (lamp and grating) and emission spectral response (detector and grating) by standard correction curves. The emission spectra of four toluene solutions of B(α)P at different concentrations (0.10, 1.0, 10, 100 mg/L) added with C_{60} fullerene (25 mg/L) - to take into account possible energy transfer phenomena occurring between B(α)P and C_{60}- were analyzed, and a calibration curve obtained by plotting the intensity maxima of the peaks (λ_{exc} = 360 nm, λ_{em} = 430 nm). Then, the B(α)P concentration was measured on three independent samples of C_{60} stock suspension contaminated with B(α)P (1 mg/L) in water, dried, and the aggregates suspended in toluene and analysed for the quantification of the B(α)P adsorbed portion (detection limit $\geq$ 0.05 mg/L).

1.2 Biomarkers analysis

Embryos were homogenized using a pestle in 100 mM potassium phosphate buffer (KCl 100 mM, EDTA 1 mM, protease inhibitors 1:100 v/v, dithiothreitol 1 mM pH 7.4). The homogenates were centrifuged at 15,000 x g for 10 minutes at 4 °C. The GST activity was measured by adding reduced glutathione (1 mM) in 100 mM phosphate buffer (pH 7.4) and using CDNB (1mM) as substrate. The reaction was monitored for 1 min at 340 nm. The CAT activity was determined by measuring the consumption of H_2O_2 (50 mM) in 100 mM potassium phosphate buffer (pH 7) at 240 nm. The SOD activity was determined by measuring the degree of inhibition of cytochrome c (10 μM) reduction by the superoxide anion generated by the xanthine oxidase (1.87 mU/mL)/hypoxanthine (50 μM) reaction at 550 nm. The activity is given as SOD units (1 SOD unit=50% inhibition of the xanthine oxidase reaction). Protein carbonyls were derivatized with 2,4-dinitrophenylhydrazine (DNPH) (10 mM in 2M HCl). Proteins were then precipitated and the pellet washed and resuspended in guanidine hydrochloride (6 M). The absorbance of protein-hydrozone was measured at 370 nm (Mecocci et al., 1999). The total protein content of each sample was measured according to the Bradford (1976) method using bovine serum albumin as standard.

Concerning biomarkers of genotoxicity, first we confirmed that the mean cell viability of dissociated cells from embryos exposed to B(α)P and C_{60} alone and combined was always higher than the threshold value (70%) suggested for the application of the genotoxicity tests (Kirkland et al., 2007). The alkaline (pH > 13) Single Cell Gel Electrophoresis (SCGE) assay was performed according to the method described in Koshmel et al. (2008). One hundred cells per slide (n = 9; three slides per each pool) were analyzed using the Comet Score® image analysis software. The apoptotic cell frequency (%) was assessed analyzing three hundred cells per slide (n=6; two slides per each pool). The frequency of micronuclei (MN‰) was calculated on 400 cells/slide (n=6; two slides per each pool) according to Pavlica et al. (2000).

2. Results

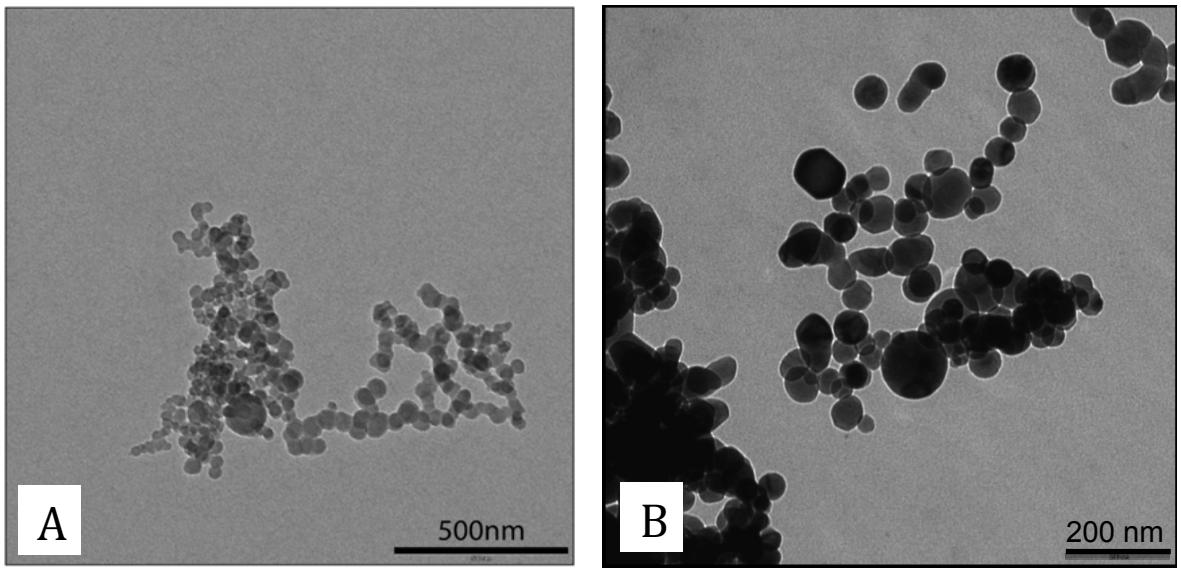

Fig. S1 TEM images of bulk C_{60} (A) and C_{60} + B(α)P (B).

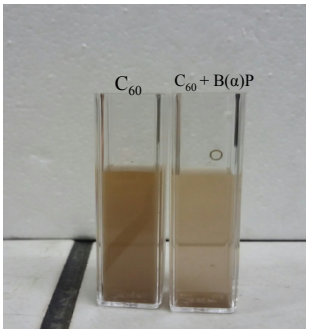

Fig. S2 Sedimentation of suspensions of C_{60} alone compared to C_{60} + B(α)P in zebrafish water.

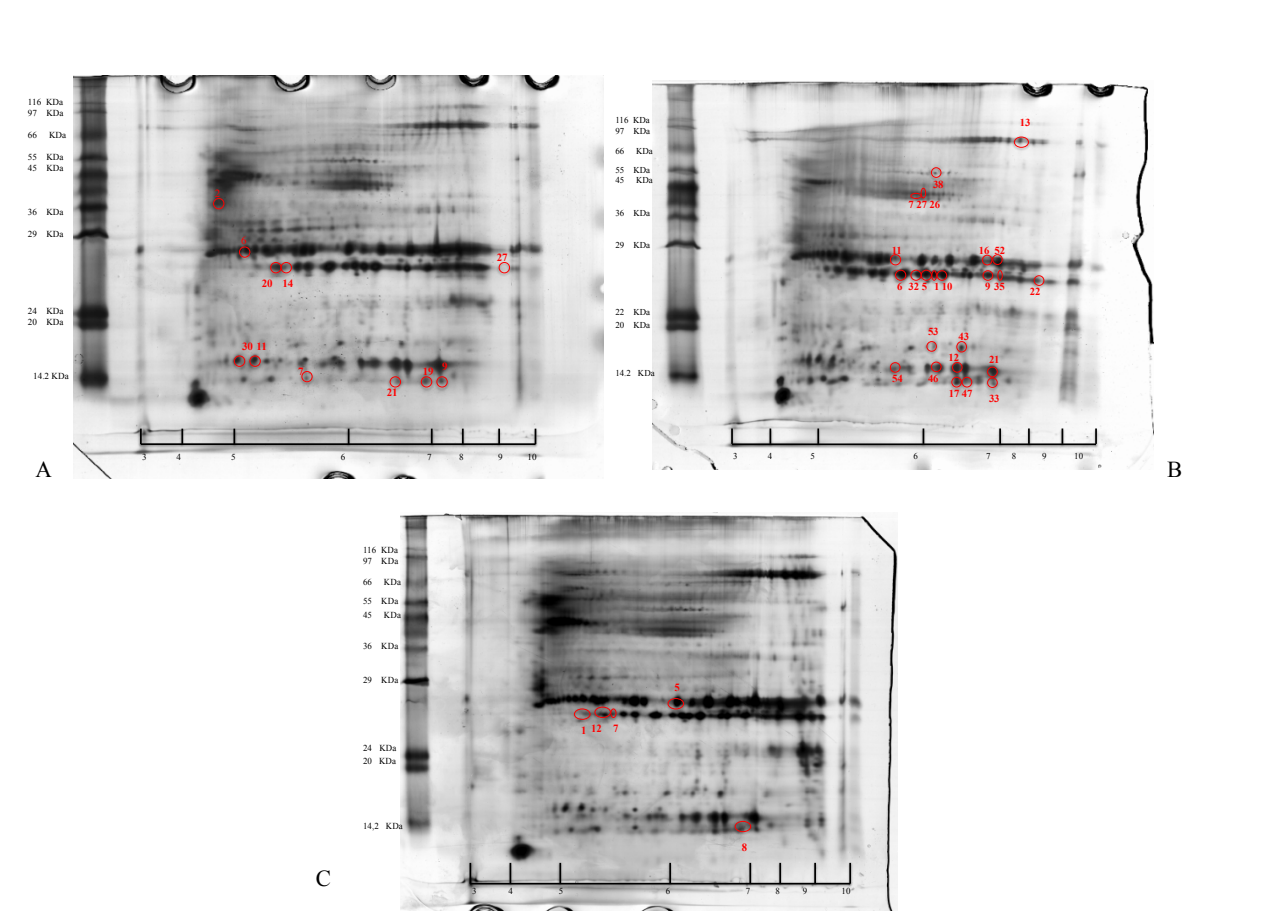

Fig. S3 Representative 2DE gels of zebrafish (96 hpf) exposed to B(α)P and C_{60} alone and C_{60} + B(α)P. Red circles highlight proteins identified through mass spectrometry analysis.

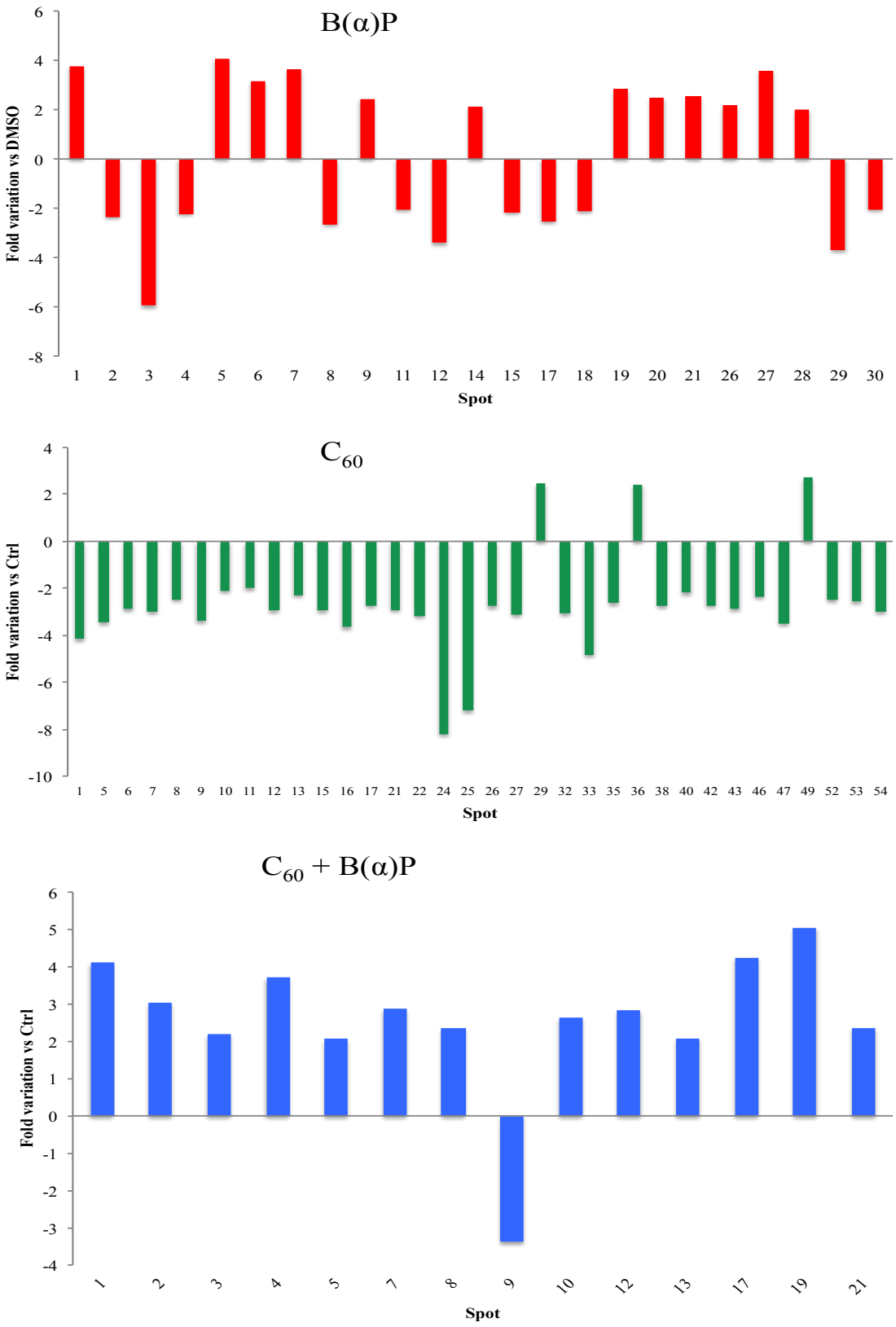

Fig. S4 Protein spots differentially expressed in zebrafish (96 hpf) exposed to B(α)P, C_{60} and C_{60} + B(α)P, with respect to controls. The *y-axis* represents the fold change (in terms of relative spot volume, % V) of the protein spots, where a positive value indicates an increase in abundance and a negative value indicates a decrease in abundance.

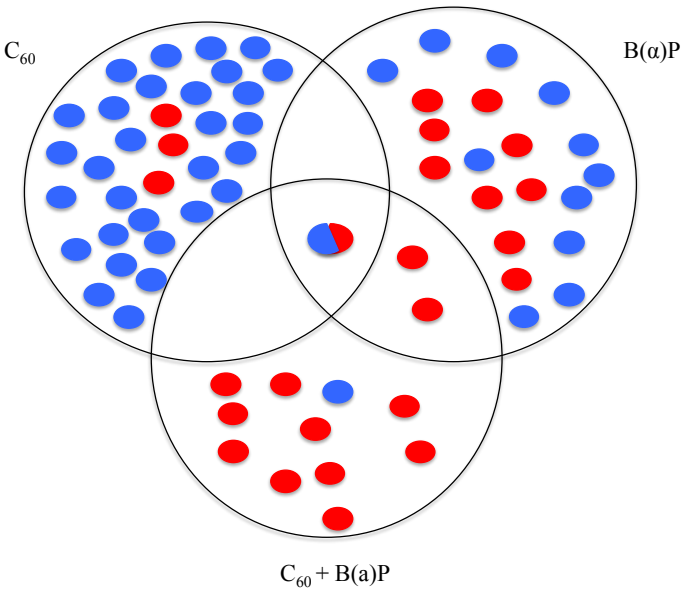

Fig. S5 Venn diagram shows common protein spots between treatments (blue=down-regulation; red=up-regulation).

References

Bradford, M., 1976. A rapid and sensitive method for the quantitation of microgram quantities of protein utilizing the principle of protein-dye binding. Analytical Biochemistry 72, 248-254.

Kirkland, D.J., Hayashi, D., Jacobson-Kram, M., Kasper, P., MacGregor, J.T., Müller, L., Uno Y. 2007. Summary of major conclusions from the 4th IWGT, San Francisco, 9–10 September. Mutat. Res., 627, 5–9.

Kosmehl, T., Hallare, A.V., Braunbeck, T., Hollert, H., 2008. DNA damage induced by genotoxicants in zebrafish (*Danio rerio*) embryos after contact exposure to freeze-dried sediment and sediment extracts from Laguna Lake (The Philippines) as measured by the comet assay. Mutation Research 650, 1-14.

Mecocci P., Fano G., Fulle S., MacGarvey U., Shinobu L., Polidori M.C., 1998. Age- dependent increases in oxidative damage to DNA, lipids, and proteins in human skeletal muscle. Free Radical Biology and Medicine 26, 303–8.

Pavlica, M., Klobucar, M., Vetma, G.I.V., Erben, N., Papeš D., 2000. Detection of micronuclei in haemocytes of zebra mussel and ramshorn snail exposed to pentachlorophenol. Mutation Research 465, 145–150.

Table S1 Proteins modified in zebrafish embryos (96 hpf) exposed to B(α)P 8 μg/L respect to DMSO

Spot[a]	Fold change (↓/↑)[b]	Protein identification	NCBInr Accession number[c]	Molecular function	Theoretical pI/MW (kDa)[d]	Experimental pI/MW (kDa)[e]	Mascot search results[f]		
							Sequence coverage (%)[g]	*N°. of matched peptides*[h]	*Score*[i]
2	2.3↓	Type I cytokeratin. enveloping layer (Cyt1) *[Danio rerio]*	AAH65653.1	Structural molecule activity	46.53/5.13	41.36/4.7	15	6/11	68
6	3.2↑	Apolipoprotein A-I precursor (Apoa1b) *[Danio rerio]*	NP_001093614.2	Lipid transport	30.18/6.05	30.56/5.1	28	7/11	78
7	3.6↑	Hemoglobin beta embryonic-1.1 (BE1) *[Danio rerio]*	NP_932339.1	Oxygen transport	16.27/6.89	13.19/5.7	29	4/4	84
9	2.5↑	Hemoglobin beta embryonic-1.1 (BE1) *[Danio rerio]*	NP_932339.1	Oxygen transport	16.27/6.89	13.19/7.3	29	4/6	73
11	2.0↓	Fatty acid binding protein 7, brain, a (Fabp7a) *[Danio rerio]*	NP_571680.1	Lipid transport	14.97/5.43	15.09/5.3	40	5/16	70
14	2.9↑	Vitellogenin 1 (Vtg 1) *[Danio rerio]*	AAH94995.1	Lipid transport	36.58/ 9.23	27.40/5.5	30	7/10	109
19	2.8↑	Hemoglobin beta embryonic-1.1 (BE1) *[Danio rerio]*	NP_932339.1	Oxygen transport	16.27/6.89	13.19/6.9	29	4/4	84
20	2.5↑	Vitellogenin 1 (Vtg 1) *[Danio rerio]*	AAH94995.1	Lipid transport	36.58/ 9.23	27.40/5.3	24	7/10	101
21	2.5↑	Hemoglobin beta embryonic-1.1 (BE1) *[Danio rerio]*	NP_932339.1	Oxygen transport	16.27/6.89	13.19/6.7	29	4/4	84
27	3.6↑	Vitellogenin 1 (Vtg 1) *[Danio rerio]*	AAH94995.1	Lipid transport	36.58/ 9.23	28.10/9.2	26	7/21	72
30	2.0↓	Vitellogenin 5 (Vtg 5) *[Danio rerio]*	AAH97081.1	Lipid transport	150/8.77	15.09/5.2	12	12/32	67

[a] ID number of spot on 2-DE map;
[b] fold change increase (↑) or decrease (↓) in terms of relative spot volume (%V) in comparison with control (DMSO).
[c] from www.uniprot.org site;

[d] Predicted p*I* and MW according to protein sequence;
[e] Experimentally determined p*I* and MW;
[f] Results obtained by Peptide Mass Fingerprinting analysis;
[g] Percentage of sequence coverage of matched peptides in the identified proteins;
[h] number of matched peptide/total number of peptide searched;
[i] probabilistic score sorted by the software (protein scores greater than 60 were indicated as significant. $p<0.05$. by the program)

Table S2 Proteins modified in zebrafish embryos (96 hpf) exposed to C_{60} 20 mg/L respect to Ctrl

Spot[a]	Fold change (↓/↑)[b]	Protein identification	NCBInr Accession number[c]	Molecular function	Theoretical pI/MW (kDa)[d]	Experimental pI/MW (kDa)[e]	Mascot search results[f]		
							Sequence coverage (%)[g]	*N°. of matched peptides*[h]	*Score*[i]
1	4.0↓	Vitellogenin 1 (Vtg 1) *[Danio rerio]*	AAH94995.1	Lipid transport	36.58/ 9.23	27.67/6.1	37	13/27	151
5	3.5↓	Vitellogenin 1 (Vtg 1) *[Danio rerio]*	AAH94995.1	Lipid transport	36.58/ 9.23	27.67/6.0	38	12/22	150
6	2.9↓	Vitellogenin 1 (Vtg 1) *[Danio rerio]*	AAH94995.1	Lipid transport	36.58/ 9.23	27.67/5.8	48	18/43	167
7	3.0↓	Muscle creatine kinase a (Ckma) *[Danio rerio]*	NP_571007.2	Kinase activity ATP binding	43/6.32	44.39/6.3	32	11/17	140
9	3.4↓	Vitellogenin 1 (Vtg 1) *[Danio rerio]*	AAH94995.1	Lipid transport	36.58/ 9.23	27.67/6.8	39	13/29	135
10	2.1↓	Vitellogenin 1 (Vtg 1) *[Danio rerio]*	AAH94995.1	Lipid transport	36.58/ 9.23	27.67/6.2	41	13/31	144
11	2.0↓	Apolipoprotein A-I precursor (Apoa1b) *[Danio rerio]*	NP_001093614.2	Lipid transport	30.18/6.05	30.68/5.9	18	5/7	58
12	3.0↓	Vitellogenin 1 (Vtg 1) *[Danio rerio]*	AAK94945.1	Lipid transport	159/ 8.68	16.25/6.4	11	10/13	99
13	2.3↓	Vitellogenin 1 precursor (Vtg 1) *[Danio rerio]*	NP_001038362.3	Lipid transport	151/8.74	77.95/8	19	23/35	170
16	3.7↓	Vitellogenin 1	AAI39514.1	Lipid transport	117/ 9.07	30.68/6.9	13	10/23	67

		(Vtg 1) *[Danio rerio]*							
17	2.7↓	Hemoglobin beta embryonic-1.1 (BE1) *[Danio rerio]*	NP_932339.1	Oxygen transport	16.27/6.89	14.87/6.5	29	4/9	64
20	3.2↓	Hemoglobin beta embryonic-1.1 (BE1) *[Danio rerio]*	NP_932339.1	Oxygen transport	16.27/6.89	13.19/6.7	29	4/4	84
21	3.2↓	Vitellogenin 1 (Vtg 1) *[Danio rerio]*	AAK94945.1	Lipid transport	150/ 8.68	16.25/7	10	11/21	81
22	8.1↓	Vitellogenin 1 (Vtg 1) *[Danio rerio]*	AAH94995.1	Lipid transport	36.58/ 9.23	27.26/8.3	36	10/21	117
24	7.2↓	Vitellogenin 7 (Vtg7) *[Danio rerio]*	AAW56971.1	Lipid transport	24.49/ 8.37	28.50/ 7.9	49	12/21	182
26	2.8↓	muscle-specific creatine kinase (Ckma) *[Danio rerio]*	AAK64515.1	Kinase activity ATP binding	43.03/6.32	45.05/6.3	26	9/13	113
27	2.8↓	muscle-specific creatine kinase (Ckma) *[Danio rerio]*	AAK64515.1	Kinase activity ATP binding	43.03/6.32	45.05/6.3	27	9/16	103
32	3.1↓	Vitellogenin 1 (Vtg 1) *[Danio rerio]*	AAH94995.1	Lipid transport	36.58/ 9.23	27.67/5.8	38	10/17	131
33	4.9↓	Hemoglobin beta embryonic-1.1 (BE1) *[Danio rerio]*	NP_932339.1	Oxygen transport	16.27/6.89	14.87/6.9	34	5/9	84
35	2.6↓	Vitellogenin 1 (Vtg 1) *[Danio rerio]*	AAH94995.1	Lipid transport	36.58/ 9.23	27.67/7.3	27	7/18	78
38	3.0↓	creatine kinase M-type isoform X1 (Ckmb) *[Danio rerio]*	XP_005157650.1	Kinase activity ATP binding	43.11/6.29	48.50/6.3	18	6/7	84
43	3.0↓	nucleoside diphosphate kinase B (Nme2b.2)	NP_571002.1	ATP binding	17.23/6.75	18.56/6.7	56	8/12	117
46	2.3↓	Vitellogenin 1 (Vtg 1) *[Danio rerio]*	AAK94945.1	Lipid transport	150/ 8.68	16.01/6.2	9	9/14	79
47	3.3↓	Hemoglobin beta embryonic-1.1 (BE1) *[Danio rerio]*	NP_932339.1	Oxygen transport	16.27/6.89	14.87/6.5	43	5/10	83
52	2.3↓	Vitellogenin 1 precursor (Vtg 1) *[Danio rerio]*	NP_001038362.3	Lipid transport	150/8.74	30.68/7	12	12/34	63

53	2.7↓	nucleoside diphosphate kinase B (Nme2b.2)	NP_571002.1	ATP binding	17.23/6.75	18.56/6.2	37	4/6	71
54	3.0↓	Vitellogenin 1 (Vtg 1) *[Danio rerio]*	AAK94945.1	Lipid transport	150/ 8.68	16.25/5.8	8	8/12	73

[a] ID number of spot on 2-DE map;
[b] fold change increase (↑) or decrease (↓) in terms of relative spot volume (%V) in comparison with control (ZFW).
[c] from www.uniprot.org site;
[d] Predicted p*I* and MW according to protein sequence;
[e] Experimentally determined p*I* and MW;
[f] Results obtained by Peptide Mass Fingerprinting analysis;
[g] Percentage of sequence coverage of matched peptides in the identified proteins;
[h] number of matched peptide/total number of peptide searched;
[i] probabilistic score sorted by the software (protein scores greater than 60 were indicated as significant. $p<0.05$. by the program)

Table S3 Proteins modified in zebrafish embryos (96 hpf) exposed to C_{60} 20 mg/L + B(α)P 8 μg/L respect to Ctrl

***Spot*[a]**	**Fold change (↓/↑)[b]**	**Protein identification**	**NCBInr Accession number[c]**	**Molecular function**	**Theoretical pI/MW (kDa)[d]**	**Experimental pI/MW (kDa)[e]**	**Mascot search results[f]**		
							***Sequence coverage* (%)[g]**	***N°. of matched peptides*[h]**	***Score*[i]**
1	4.1↑	Vitellogenin 1 (Vtg 1) *[Danio rerio]*	AAH94995.1	Lipid transport	36.58/ 9.23	27.40/5.2	30	9/18	112
5	4.1↑	Vitellogenin 1 (Vtg 1) *[Danio rerio]*	AAI39514.1	Lipid transport	117/ 9.07	30.7/6	10	7/12	93
7	2.9↑	Vitellogenin 1 (Vtg 1) *[Danio rerio]*	AAI39514.1	Lipid transport	117/ 9.07	27.40/5.5	30	7/10	109
8	2.4↑	Hemoglobin beta embryonic-1.1 (BE1) *[Danio rerio]*	NP_932339.1	Oxygen transport	16.27/6.89	13.19/6.7	29	4/4	84
12	2.8↑	Vitellogenin 1 (Vtg 1) *[Danio rerio]*	AAH94995.1	Lipid transport	36.58/ 9.23	27.40/5.3	24	7/10	101

[a] ID number of spot on 2-DE map;
[b] fold change increase (↑) or decrease (↓) in terms of relative spot volume (%V) in comparison with control (ZFW).
[c] from www.uniprot.org site;

[d] Predicted p*I* and MW according to protein sequence;
[e] Experimentally determined p*I* and MW;
[f] Results obtained by Peptide Mass Fingerprinting analysis;
[g] Percentage of sequence coverage of matched peptides in the identified proteins;
[h] number of matched peptide/total number of peptide searched;
[i] probabilistic score sorted by the software (protein scores greater than 60 were indicated as significant. $p<0.05$. by the program)